ARMY RESEARCH LABORATORY

Control Authority of a Projectile Equipped With an Internal Unbalanced Part

by Geoffrey W. Frost and Mark F. Costello

ARL-CR-555 **November 2004**

NOTICES

Disclaimers

The findings in this report are not to be construed as an official Department of the Army position unless so designated by other authorized documents.

Citation of manufacturer's or trade names does not constitute an official endorsement or approval of the use thereof.

Destroy this report when it is no longer needed. Do not return it to the originator.

Army Research Laboratory
Aberdeen Proving Ground, MD 21005-5066

ARL-CR-555 **November 2004**

Control Authority of a Projectile Equipped With an Internal Unbalanced Part

Geoffrey W. Frost and Mark F. Costello
Oregon State University

REPORT DOCUMENTATION PAGE	Form Approved OMB No. 0704-0188

1. REPORT DATE *(DD-MM-YYYY)*	2. REPORT TYPE	3. DATES COVERED (From - To)
November 2004	Final	October 2003–September 2004

4. TITLE AND SUBTITLE
Control Authority of a Projectile Equipped With an Internal Unbalanced Part

5a. CONTRACT NUMBER
W911QX-04-P-0270

5b. GRANT NUMBER

5c. PROGRAM ELEMENT NUMBER

6. AUTHOR(S)
Geoffrey W. Frost[*] and Mark F. Costello[†]

5d. PROJECT NUMBER
622618.H80000

5e. TASK NUMBER

5f. WORK UNIT NUMBER

7. PERFORMING ORGANIZATION NAME(S) AND ADDRESS(ES)
Oregon State University
Corvallis, OR 97331

8. PERFORMING ORGANIZATION REPORT NUMBER

9. SPONSORING/MONITORING AGENCY NAME(S) AND ADDRESS(ES)
U.S. Army Research Laboratory
ATTN: ARMSRD-ARL-WM-BC
Aberdeen Proving Ground, MD 21005-5066

10. SPONSOR/MONITOR'S ACRONYM(S)

11. SPONSOR/MONITOR'S REPORT NUMBER(S)
ARL-CR-555

12. DISTRIBUTION/AVAILABILITY STATEMENT
Approved for public release; distribution is unlimited.

13. SUPPLEMENTARY NOTES
[*]Graduate Research Assistant, Department of Mechanical Engineering, Oregon State University.
[†]Associate Professor, Department of Mechanical Engineering, Oregon State University.

14. ABSTRACT

A key technical challenge for smart weapon developers is design of appropriate control mechanisms that provide sufficient control authority to enable correction of typical trajectory errors while not excessively burdening the overall weapon design. The work reported here considers a rotating mass unbalance control mechanism created by radial orientation of an internal part. To investigate the potential of this control mechanism, a seven degree-of-freedom flight dynamic model of a projectile equipped with an internal part is defined. Using this dynamic model, it is shown that by holding the internal part fixed with respect to a nonrolling reference frame, predictable trajectory changes are generated, including predictable impact point changes. As expected, when unbalance-offset distance or mass is increased, control authority increases proportionally. This control mechanism is capable of creating impact point changes that are the same order of magnitude as dispersion caused by errors induced at launch and in flight. To achieve this level of control authority, the projectile must be designed less stable than is typical of conventional uncontrolled fin and spin-stabilized projectiles.

15. SUBJECT TERMS
guided projectile, divert control, unbalanced part

16. SECURITY CLASSIFICATION OF: UNCLASSIFIED			17. LIMITATION OF ABSTRACT	18. NUMBER OF PAGES	19a. NAME OF RESPONSIBLE PERSON
a. REPORT	b. ABSTRACT	c. THIS PAGE			Peter Plostins
UNCLASSIFIED	UNCLASSIFIED	UNCLASSIFIED	UL	60	19b. TELEPHONE NUMBER (*Include area code*) 410-278-8878

Standard Form 298 (Rev. 8/98)
Prescribed by ANSI Std. Z39.18

Contents

List of Figures

INTENTIONALLY LEFT BLANK.

1. Introduction

As the range of uncontrolled weapons is increased, a side effect is a concomitant increase in impact point dispersion. To statistically neutralize a target, the number of rounds to be fired by a conventional weapons system is directly proportional to the impact point dispersion of the system. Thus, the price to pay for increased projectile range is firing more rounds at the target (*1*, *2*). To circumvent this basic limitation of conventional weapon systems, designers are considering employing active control technology to simultaneously enable both increased range and decreased dispersion for future systems. A key component of a smart projectile is the control mechanism. The control mechanism must be capable of altering the trajectory of the projectile in such a way that impact point errors induced at launch and in flight can be corrected. At the same time, the control mechanism must be rugged (to withstand high acceleration loads at launch), small (so that payload space is not compromised), and inexpensive (for cost considerations).

Current projectile control mechanisms include configurations capable of manipulating aerodynamic loads, generating jet thrust, and altering inertial loads on the body. Examples of aerodynamic control mechanisms include rotation of aerodynamic lifting surface appendages, deflection of the nose, and deflection of ram air to side ports. Examples of jet thrust control mechanisms include gas jet and explosive thrusters. Examples of inertial control mechanisms include internal translation of a control mass and internal rotation of an unbalanced part.

Many conventional uncontrolled projectile configurations contain internal parts that move slightly in flight. For example, submunitions deployed from indirect fire projectiles are keyed into place inside the round; however, small relative motion occurs. Also, fuze mechanisms used on some indirect fire ammunition employ a rotor that is permitted to move slightly with respect to the main projectile body. Although seemingly insignificant from a dynamic modeling perspective, small mass unbalances in these configurations can induce instability of the round as a whole, typified in flight by a large loss in range and large spin decay. For this reason, several researchers have investigated dynamic stability of projectiles with moving internal components (*3*). Soper (*4*) evaluated the stability of a spinning projectile that contains a cylindrical mass fitted loosely into a cylindrical cavity. Using a similar geometric configuration, Murphy (*5*) developed a quasilinear solution for a projectile with an internal moving part. Later, D'Amico (*6*) performed a detailed series of experiments where a projectile with a loose internal part was driven by the rotor of a freely gimbaled gyroscope. Hodapp (*7*) expanded the work of Soper and Murphy by considering a projectile configuration with a partially restrained internal member with a mass center offset.

Some new projectile configurations are designed with sizeable moving parts that are fundamental to the operation of the projectile. For example, the gimbal nose projectile configuration mounts

the nose section on a gimbal joint so that the nose is capable of rotating freely with respect to the main body of the projectile. Several investigations have evaluated the potential of the gimbal nose concept to be used as a control mechanism and a means to reduce dispersion (*8–10*). Another example of a multiple component configuration is the dual-spin projectile, which consists of forward and aft sections connected through a bearing, allowing different spin rates for each section. The utility of the configuration has emerged for guided spin-stabilized rounds where the control mechanism is isolated from the rapidly rotating main body (*11–13*).

The work reported here evaluates control authority of fin-stabilized and spin-stabilized projectiles equipped with an internal part that can be controlled to an arbitrary roll orientation. At launch, the part is assumed to be symmetric and located on the projectile axis of symmetry in order to avoid trajectory changes due to lateral throw-off. Before the control mechanism is deployed, it is rotated to the desired roll orientation. The unbalance is subsequently deployed, yielding an unbalanced configuration. By holding the part in different roll orientations with respect to a nonrolling reference frame, predictable trajectory changes occur, suggesting a potential control mechanism. The effects of varying inertia and aerodynamic properties of a nominal rigid projectile are studied. The report begins with the description of a seven degree-of-freedom (DOF) flight dynamic model used for trajectory predictions along with the description of a flight control system to track commanded roll orientation of the part. The model is subsequently employed to predict control authority of exemplary fin-stabilized and spin-stabilized projectiles and of the same projectiles modified such that their inertia and aerodynamic properties are more responsive to control. Control authority vs. the radial offset, activation time, mass of unbalance, and system velocity is documented.

2. Internal Part Projectile Dynamic Model

A projectile containing an internal part and a mechanism capable of actively controlling the angular position of that part about its axle is considered as shown in figure 1. The projectile (*P*) and the internal part (*D*) are both rigid bodies connected at an arbitrary point (*C*). The motion of the part is constrained to rotate about its axle. Figure 1 shows the relative locations of the centers of gravity for the projectile, part, and initially symmetrical system (*S*). The mathematical model describing the motion of the system allows for seven rigid-body DOFs. Three translational and three rotational DOFs are used to describe the motion of the main body, and one rotational DOF is used to describe the angular motion of the part with respect to the main projectile body. In order to develop the dynamic equations of motion for these seven DOFs, three separate reference frames are used, as shown in figure 1. The ground surface is used as an inertial reference frame with $\vec{K}_I$ positive down. A body frame is fixed on the projectile at the system reference point with $\vec{I}_P$ positive out the nose of the projectile. Another body frame is fixed on the center of the part bearing and its axle such that $\vec{I}_D$ lies along the axle of the part.

The part body frame is initially coincident with the projectile body frame and is oriented with respect to the projectile body frame through a set of body-fixed rotations, ψ_D, θ_D, and ϕ_D. The transformations are obtained using the standard aerodynamic rotation sequence described by Etkin (*13*).

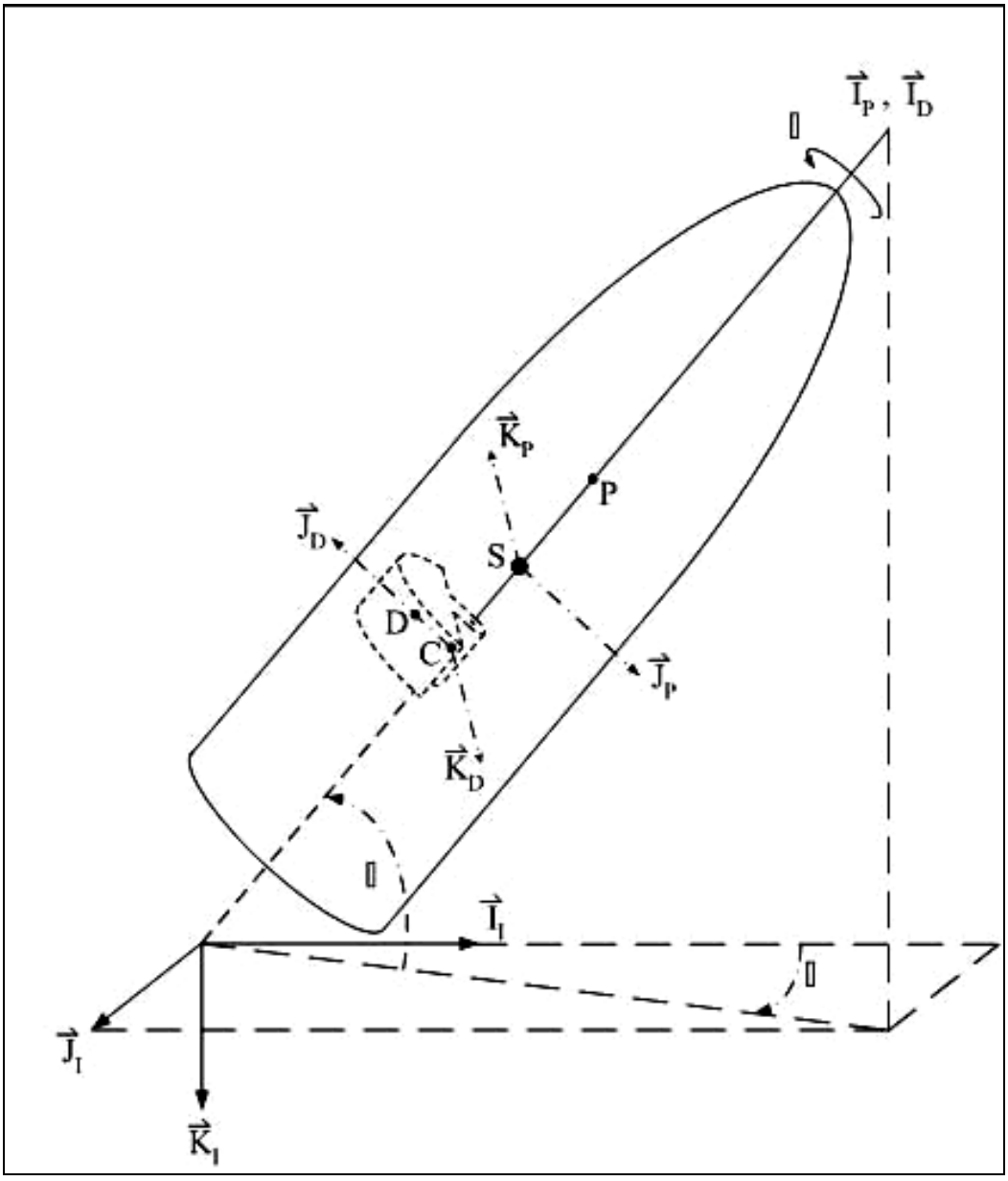

Figure 1. Example system configuration.

Applying the projectile body frame to inertial frame transformation to the mass center velocity vector yields the translational kinematic differential equations:

$$\begin{Bmatrix} \dot{x} \\ \dot{y} \\ \dot{z} \end{Bmatrix} = T_P \begin{Bmatrix} u \\ v \\ w \end{Bmatrix}. \tag{1}$$

$$T_P = \begin{bmatrix} c_\theta c_\psi & s_\phi s_\theta c_\psi - c_\phi s_\psi & c_\phi s_\theta c_\psi + s_\phi s_\psi \\ c_\theta s_\psi & s_\phi s_\theta s_\psi + c_\phi c_\psi & c_\phi s_\theta s_\psi - s_\phi c_\psi \\ -s_\theta & s_\phi c_\theta & c_\phi c_\theta \end{bmatrix}. \tag{2}$$

Equating the angular velocity components, using Euler angle time derivatives and body frame angular velocity components, yields the rotational kinematic differential equations:

$$\begin{Bmatrix} \dot{\phi} \\ \dot{\theta} \\ \dot{\psi} \\ \dot{\phi}_D \end{Bmatrix} = \begin{bmatrix} 1 & s_\phi t_\theta & c_\phi t_\theta & 0 \\ 0 & c_\phi & -s_\phi & 0 \\ 0 & s_\phi / c_\phi & c_\phi / c_\theta & 0 \\ 0 & 0 & 0 & 1 \end{bmatrix} \begin{Bmatrix} p \\ q \\ r \\ \omega \end{Bmatrix}. \tag{3}$$

The kinematic differential equations define seven of the fourteen dynamic equations needed to describe the trajectory of the states. The remaining seven differential equations are derived by separating the two-body system at the part axle connection point and considering the reaction forces and moments associated with each individual body, as shown in figure 2.

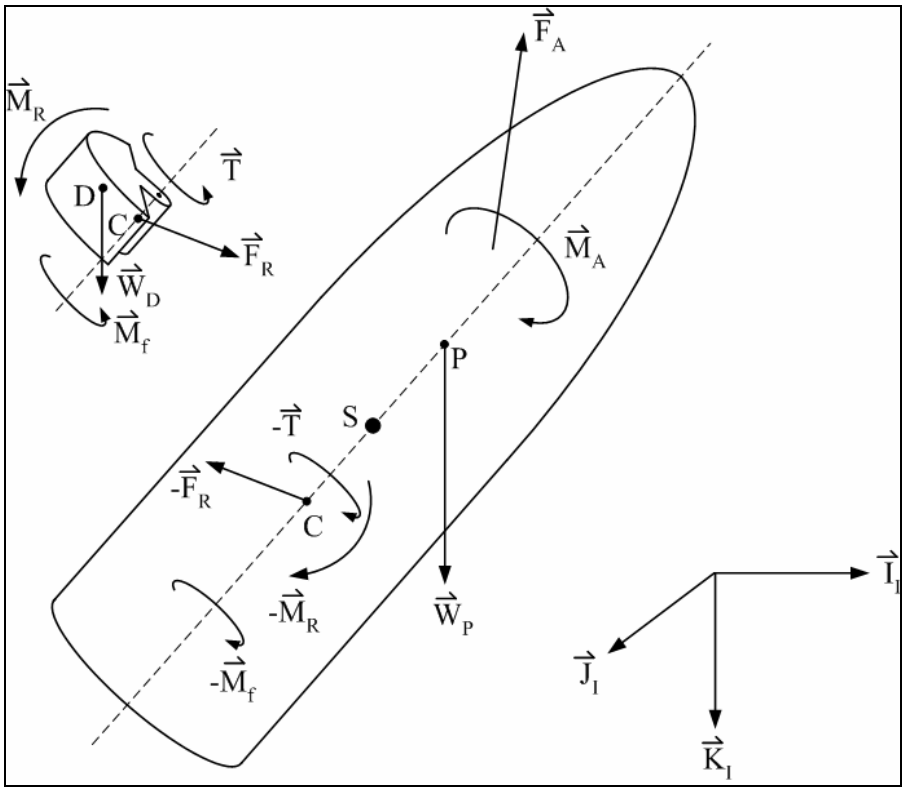

Figure 2. Free body diagram.

A constraint force, $\vec{F}_R$, and a constraint moment, $\vec{M}_R$, applied at the connection point *C* couple the part and projectile bodies. Axial moments, $\vec{T}$ and $\vec{M}_F$, due to torque generated by the controlling mechanism and bearing friction are applied to the bodies. The projectile body is also acted on by aerodynamic forces, $\vec{F}_A$, and aerodynamic moments, $\vec{M}_A$. The translational dynamic equations of motion for each body are given in equations 4 and 5:

$$m_D \vec{a}_{D/I} = \vec{F}_R + \vec{W}_D . \tag{4}$$

$$m_P \vec{a}_{P/I} = -\vec{F}_R + \vec{W}_P + \vec{F}_A . \tag{5}$$

Summing equations 4 and 5 eliminates the reaction force and yields the translational dynamic equation of motion for the projectile. When expressed in component form in the projectile body frame, it yields three translational kinetic differential equations:

$$m_P \vec{a}_{P/I} + m_D \vec{a}_{D/I} = \vec{W}_D + \vec{W}_P + \vec{F}_A . \tag{6}$$

The acceleration of the mass center of the projectile $\vec{a}_{P/I}$ is expressed in terms of the acceleration of the stationary system reference point, *S*, by applying the formula for two points fixed on a rigid body from the stationary system reference point to the projectile mass center:

$$\vec{a}_{P/I} = \vec{a}_{S/I} + \vec{\alpha}_{P/I} \times \vec{r}_{S\to P} + \vec{\omega}_{P/I} \times (\vec{\omega}_{P/I} \times \vec{r}_{S\to P}), \tag{7}$$

where

$$\vec{a}_{S/I} = \frac{{}^{P}d\vec{V}_{S/I}}{dt} + \vec{\omega}_{P/I} \times \vec{V}_{S/I} . \tag{8}$$

The acceleration of the mass center of the part $\vec{a}_{D/I}$ is expressed in terms of the acceleration of the stationary system reference point, *S*, by applying the formula for two points fixed on a rigid body from the stationary system reference point to the connection joint *C*, and again from the connection joint to the part mass center *D*:

$$\begin{aligned} \vec{a}_{D/I} = {} & \vec{a}_{S/I} + \vec{\alpha}_{P/I} \times \vec{r}_{S\to C} + \vec{\omega}_{P/I} \times (\vec{\omega}_{P/I} \times \vec{r}_{S\to C}) \\ & + \vec{\alpha}_{D/I} \times \vec{r}_{C\to D} + \vec{\omega}_{D/I} \times (\vec{\omega}_{D/I} \times \vec{r}_{C\to D}). \end{aligned} \tag{9}$$

The angular accelerations with respect to the inertial frame of the projectile body, $\vec{\alpha}_{P/I}$, and the part body, $\vec{\alpha}_{D/I}$, is found by taking the derivatives of the respective angular velocities:

$$\frac{{}^{I}d\vec{\alpha}_{P/I}}{dt} = \frac{{}^{P}d\vec{\omega}_{P/I}}{dt} + \vec{\omega}_{P/I} \times \vec{\omega}_{P/I} . \tag{10}$$

$$\frac{{}^{I}d\vec{\alpha}_{D/I}}{dt} = \frac{{}^{P}d\vec{\omega}_{P/I}}{dt} + \frac{{}^{P}d\vec{\omega}_{D/P}}{dt} + \vec{\omega}_{P/I} \times \left(\vec{\omega}_{P/I} + \vec{\omega}_{D/P}\right). \tag{11}$$

Summing the moments acting on the part about the connection point *C* yields the rotational equation of motion for the part body. The rotational dynamic equation of motion for the projectile body is found by summing the moments about the projectile mass center:

$$ {}^{I}\frac{d\vec{H}_{D/I}}{dt} + \vec{r}_{C\to D}\times\vec{a}_{D/I} = \vec{T} + \vec{M}_R + \vec{r}_{C\to D}\times\vec{W}_D - \vec{M}_F . \tag{12} $$

$$ \frac{{}^{I}d\vec{H}_{P/I}}{dt} = \vec{M}_A - \vec{T} - \vec{M}_R - \vec{r}_{P\to C}\times\vec{F}_R + \vec{M}_F . \tag{13} $$

Summing equations 12 and 13 eliminates the reaction moments and forms the rotational dynamic equation of motion for the two-body system. This equation yields three rotational kinetic differential equations. In component form, it is expressed in the projectile body frame:

$$ \frac{{}^{I}d\vec{H}_{P/I}}{dt} + \frac{{}^{I}d\vec{H}_{D/I}}{dt} = \vec{M}_A - \vec{r}_{C\to D}\times\vec{a}_{D/I} - \vec{r}_{P\to C}\times\vec{F}_R + \vec{r}_{C\to D}\times\vec{W}_D . \tag{14} $$

The constraint force is obtained by subtracting equation 5 from equation 4:

$$ \vec{F}_R = \left(\vec{a}_{D/I} - \vec{a}_{P/I} + \frac{\vec{F}_A}{m_P}\right)\left(\frac{m_D m_P}{m_D + m_P}\right). \tag{15} $$

The aerodynamic loads $\vec{F}_A$ and moments $\vec{M}_A$ exerted on the projectile body in the previous equations are found using standard aerodynamic theory for projectiles (*14*).

The derivatives of angular momentum of the bodies are given in equations 16 and 17:

$$ {}^{I}\frac{d\vec{H}_{D/I}}{dt} = {}^{P}\frac{d\vec{H}_{D/I}}{dt} + \vec{\omega}_{P/I}\times\vec{H}_{D/I} . \tag{16} $$

$$ \frac{{}^{I}d\vec{H}_{P/I}}{dt} = {}^{P}\frac{d\vec{H}_{P/I}}{dt} + \vec{\omega}_{P/I}\times\vec{H}_{P/I} . \tag{17} $$

The final kinetic differential equation is found by summing the axial moments acting on the part. This is accomplished by dotting each term of the rotational dynamic equation of motion of the part body with the unit vector $\vec{I}_D$ of the disk body frame. An axle joint cannot support an axial constraint moment, and therefore the reaction moment $\vec{M}_R$ does not appear in the equation:

$$ \vec{I}_D \bullet {}^{I}\frac{d\vec{H}_{D/I}}{dt} + \vec{I}_D \bullet \left(\vec{r}_{C\to D}\times\vec{a}_{D/I}\right) = \vec{I}_D \bullet \vec{T} + \vec{I}_D \bullet \left(\vec{r}_{C\to D}\times\vec{W}_D\right) - \vec{M}_F . \tag{18} $$

The independent state variables *x*, *y*, *z*, ϕ, θ, ψ, and ϕ_D are defined by the kinematic differential equations. The variables *u*, *v*, *w*, *p*, *q*, *r*, and ω are chosen for the remaining seven states variables and are conveniently concatenated into the vector *s*:

$$s = \{u \quad v \quad w \quad p \quad q \quad r \quad \omega\}^T . \tag{19}$$

The seven kinetic differential equations are found by expressing the dynamic equations of motion given by equations 6, 14, and 18 in component form. The body frame components of the dynamic equations of motion can be written as

$$\begin{bmatrix} A_{PT} \\ A_{PR} \\ A_{DR} \end{bmatrix} \dot{s} = \begin{Bmatrix} B_{PT} \\ B_{PR} \\ B_{DR} \end{Bmatrix} . \tag{20}$$

The matrices A_{PT}, A_{PR}, and A_{DR}, the vectors B_{PT}, B_{PR}, and B_{DR}, and the individual terms that form them are given in the appendix.

3. System Mass and Inertia Properties

To properly compare the effects on the trajectory of a projectile containing an asymmetrical internal part to that of a rigid projectile, special consideration is given to the formulation of the system's mass and inertial properties. The total mass and inertia properties of the two-component system are held constant at values equal to that of a baseline rigid projectile. A disk-shaped mass, located on the axis of symmetry of the nominal rigid projectile, is removed from the baseline rigid projectile. The removed mass is equal to that of the internal part. Resulting mass and inertia properties are appropriately modified. The modified projectile comprising the two-body system is called the projectile (*P*), and the original baseline projectile is called the nominal rigid projectile. The internal part is then added to the projectile such that if the internal part were held fixed with respect to the projectile body, the combined masses produce mass and inertia properties for the two-body system that are identical to the baseline rigid projectile. The reference point, *S*, is taken as the center of mass of the baseline rigid projectile.

4. Control Mechanism Deployment

For a gun-launched weapon, acceleration at the muzzle exit is sufficiently large to prevent proper operation of the onboard CPU until slightly after launch, as well as prevent relative motion between the projectile and internal part. If the internal part is laterally offset from the projectile axis of symmetry at the time of firing the two-body system is equivalent to a statically unbalanced projectile. A statically unbalanced projectile is mechanically constrained to rotate about its geometric center of form while traveling down a rifled gun barrel. At the muzzle of the gun, the mechanical constraint provided by the barrel is suddenly removed, and the initial conditions of the free-flight trajectory are dependent on the spin rate, the lateral offset of the

center of mass, and the roll orientation angle of the center of mass. The effect of a lateral center-of-mass offset, or static unbalance, is to change the initial direction of the trajectory of a spin-stabilized projectile at the gun muzzle (*15*). Exterior ballisticians commonly refer to this effect as lateral throw-off. Internal part offset from the projectile axis of symmetry at launch results in unpredictable changes in the trajectory because roll angle of the mass center is not practically controllable at the muzzle. To avoid lateral throw-off effects, the internal part's center of mass is located on the projectile axis of symmetry, and the part is symmetric and not spinning relative to the projectile. After the system exits the muzzle, the control-processing unit is powered on and a small amount of time is allowed to elapse in order for the system to warm up. The symmetric part is controlled to the desired roll orientation relative to a nonrolling reference frame, reformed as an asymmetrical part, and offset from the axis of symmetry inducing a stationary mass unbalance in the two-body system.

5. Internal Part Orientation Control

To affect the trajectory of the system, the roll angle of the internal part is controlled such that it causes a stationary mass unbalance of the projectile with respect to a nonrolling reference frame. Derivative control is used to reduce the spin rate of the part, defined as

$$\Omega = p + \omega, \tag{21}$$

to less than 1 rad/s. The roll orientation of the symmetric part is first controlled to the desired angle relative to the nonrolling reference frame, and then reformed asymmetrically and offset from the projectile axis of symmetry. The no-roll reference frame is located on the two-body system reference point, *S*, and is defined as an intermediate frame before roll angle rotation of the projectile body frame, as shown in figure 3. The desired control, ϕ_C, is specified as a roll angle between –180° and 180° with respect to the no-roll frame. The error, ϕ_E, is defined as the angle between the specified control angle and $\vec{J}_D$. The orientation angle of the part, ϕ_J, between $\vec{J}_D$ and $\vec{J}_N$, is given as

$$\phi_J = \phi + \phi_D. \tag{22}$$

A control reference frame is defined to be aligned with the desired part orientation angle, as shown in figure 3:

$$\begin{Bmatrix} \vec{I}_C \\ \vec{J}_C \\ \vec{K}_C \end{Bmatrix} = \begin{bmatrix} 1 & 0 & 0 \\ 0 & c_{\phi_C} & s_{\phi_C} \\ 0 & -s_{\phi_C} & c_{\phi_C} \end{bmatrix} \begin{Bmatrix} \vec{I}_N \\ \vec{J}_N \\ \vec{K}_N \end{Bmatrix}. \tag{23}$$

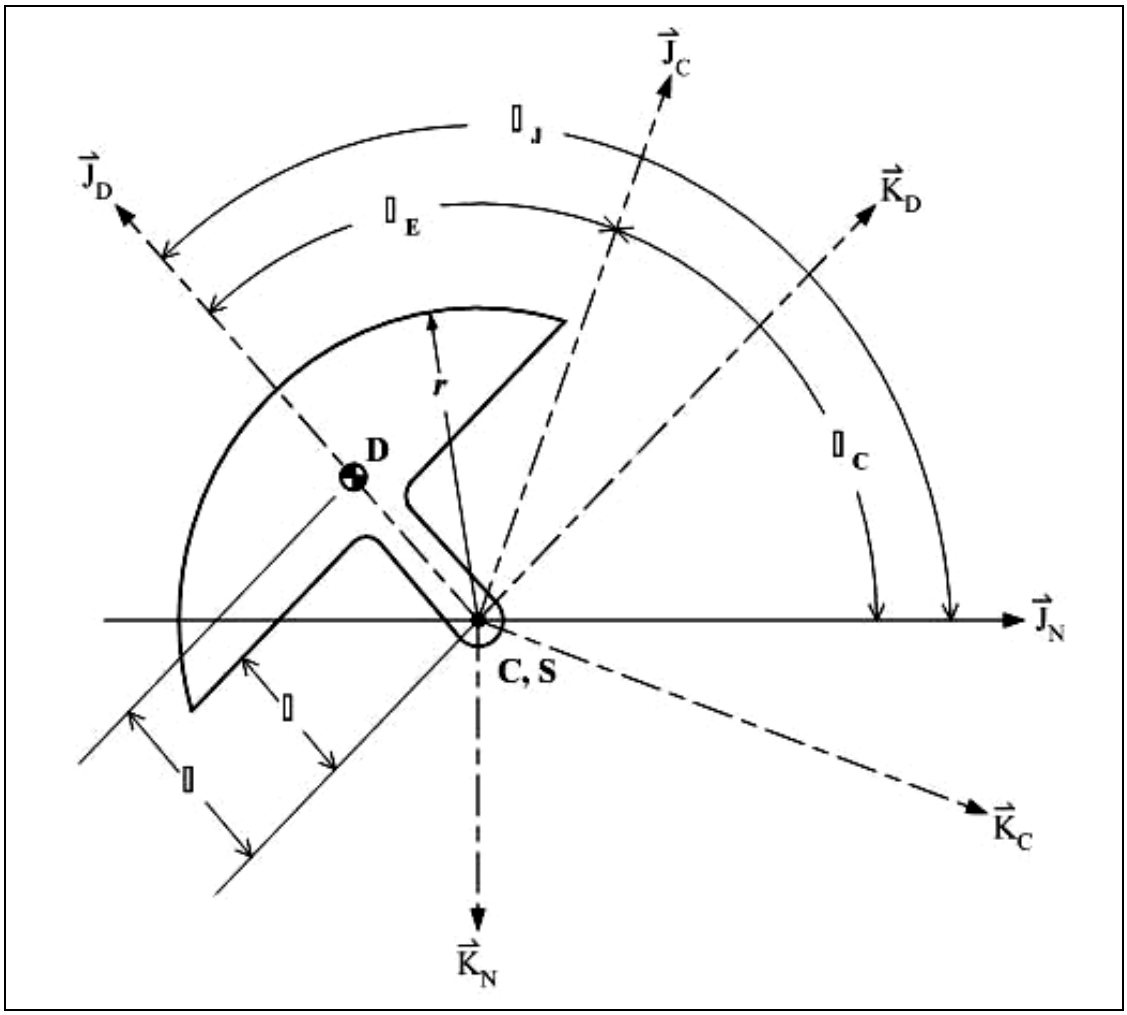

Figure 3. Internal part orientation angle control metrics.

To determine the control command, the angle of error is computed as given:

$$\phi_E = \tan^{-1}\left(\frac{s_{\phi_J} c_{\phi_C} - c_{\phi_J} s_{\phi_C}}{c_{\phi_J} c_{\phi_C} + s_{\phi_J} s_{\phi_C}}\right). \tag{24}$$

Control of the error is maintained by applying an axial torque $\vec{T}$ that is produced by the control algorithm shown in figure 4.

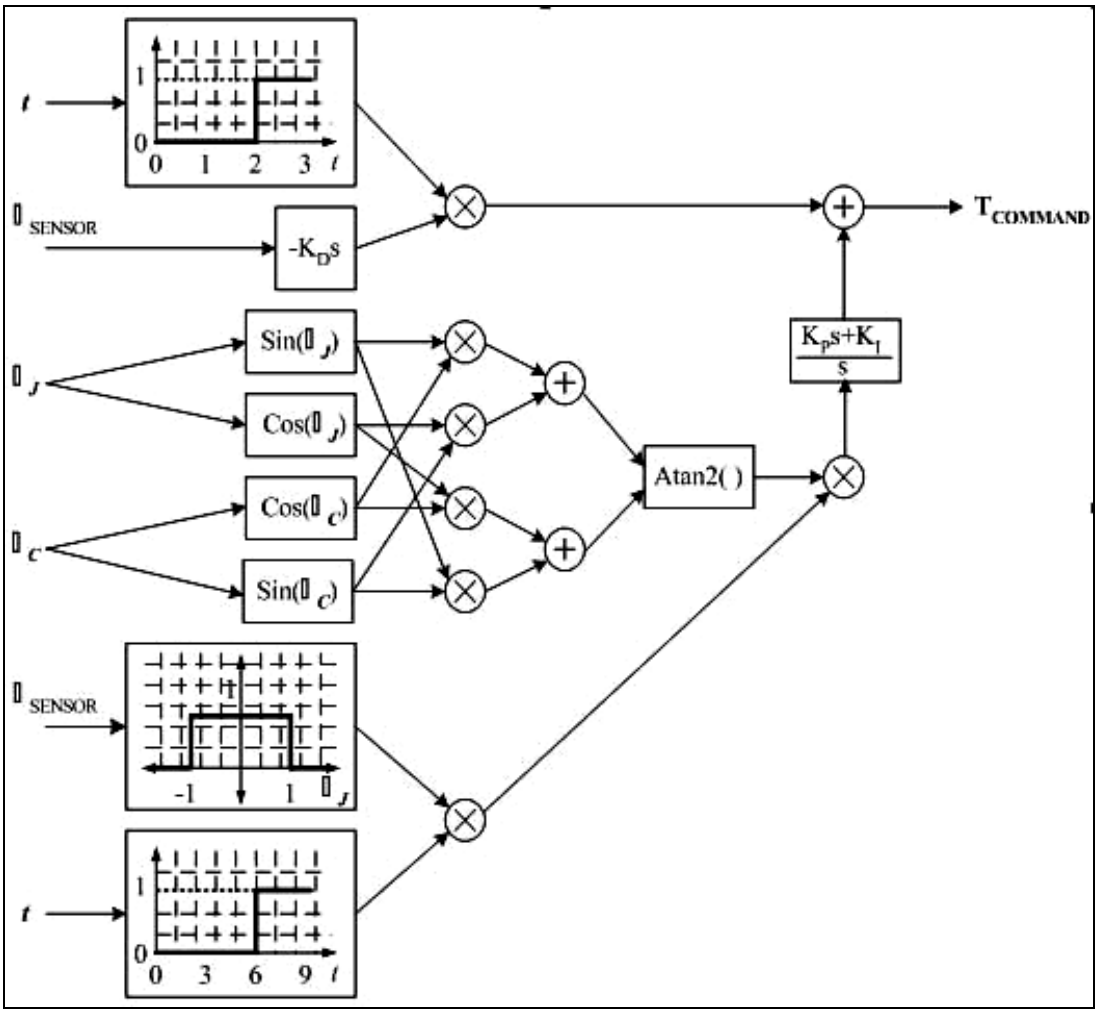

Figure 4. Internal part orientation angle and roll rate control logic.

6. Trajectory Control Mechanism

The main mechanism for steering the system is a moment produced by axial drag about the composite body center of mass that is created by positioning the part in a fixed orientation relative to the nonrolling reference frame attached to the projectile body. This moment causes a fin-stabilized system to swerve in the same direction of the resulting yawing motion. However, for a spin-stabilized system, the swerve is ~180° out of phase with the initial direction of the yaw due to the gyroscopic effects inherent in a spinning projectile. Thus, positioning the part to the right of the projectile centerline will cause a spin-stabilized system to swerve to the right and up, as shown in figure 5.

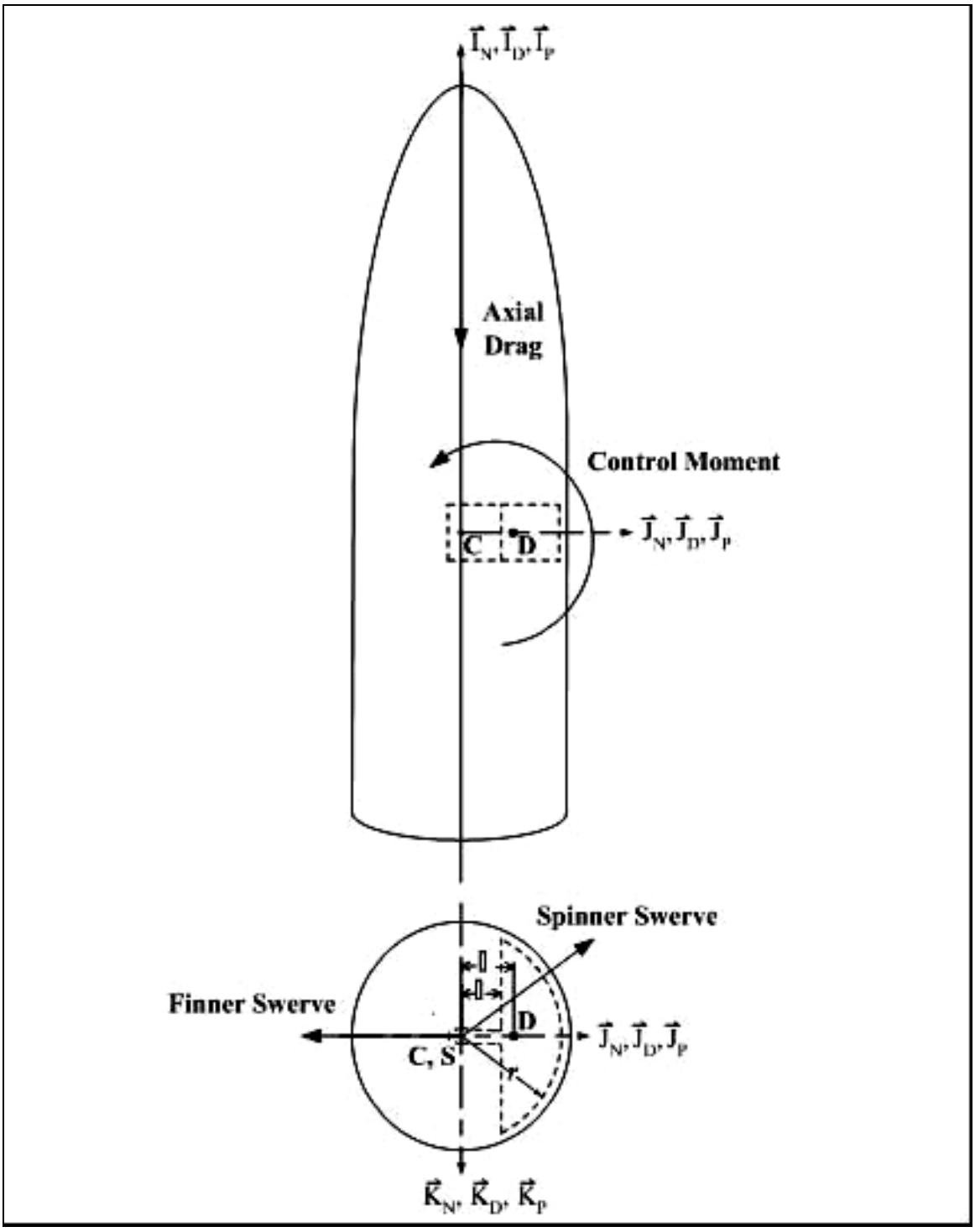

Figure 5. Trajectory control mechanism.

7. Results

To generate the trajectories, the 14 differential equations described previously are numerically integrated using a fourth-order Runge-Kutta algorithm. In order to validate the dynamic model described previously, trajectory results were generated for the special case of a symmetric disk mounted on the axis of symmetry of the projectile. Bearing friction was set sufficiently large so that relative motion between the disk and projectile was negligible, hence mimicking a rigid projectile. These trajectory results compared favorably with a well-known rigid six-DOF model driven by the same configuration data.

In the following studies, consideration is given to modifying the mass and inertia properties of the nominal rigid projectile such that it is fundamentally less stable then that of a typical fin-stabilized or spin-stabilized projectile. This modification is conducted to demonstrate the increased control authority achieved through destabilization of a nominal rigid projectile. Removing mass from the nominal rigid projectile and replacing it at a different location along the stationline alters the mass and inertia properties. For a spin-stabilized projectile, this modification shifts the nominal rigid projectile center of mass forward and closer to the aerodynamic center of pressure and decreases the resistance to rotation about the $\vec{J}_P$ and $\vec{K}_P$ projectile body axes, while maintaining the nominal rigid projectile mass. For a fin-stabilized projectile, the nominal rigid projectile center of mass is shifted aft and closer to the aerodynamic center of pressure. The seven DOF two-body system constructed with a nominal projectile is called the nominal two-body system and the seven DOF two-body system constructed with a modified projectile is called the modified two-body system. Consideration is also given to increasing the drag and lift on a modified and nominal system to further emphasize the increased control authority that is achieved by coupling this type of mechanism with nonstandard munitions. These systems are called the modified drag system and the nominal drag system.

In order to determine the effects of using an internal part as a control mechanism for a fin-stabilized projectile, the flight characteristics of a nominal, modified, and drag modified fin-stabilized system were simulated and compared to the flight characteristics of a standard rigid fin-stabilized projectile. Results are shown for a typical fin-stabilized rocket having a weight of 120.20 *N*. The nominal stationline, buttline, and waterline distances to the nominal fin-stabilized projectile center of mass are 76.2, 0, and 0 cm, respectively, measured from the base. The modified stationline, buttline, and waterline distances to the modified fin-stabilized projectile center of mass are 46.22, 0, and 0 cm, respectively, measured from the base. The nominal roll inertia is 0.025 kg-m^2, and the nominal pitch and yaw inertia is 6 kg-m^2. The fin-stabilized projectile modified roll inertia is 0.025 kg-m^2, and the modified pitch and yaw inertia is 9.95 kg-m^2. The reformed internal part consists of a semicylindrical shaped lead part mounted to an axle such that $\vec{I}_D$ coincides with $\vec{I}_P$. The semicylindrical shaped part located in the fin-

stabilized system has a radius of 3.18 cm and is 10.16 cm long. It has a mass of 1.83 kg. The part-to-projectile connection point is located at the composite body center of mass. When reformed asymmetrically, the part center of mass is radially offset from the projectile axis of symmetry a distance of $\varepsilon = 1.35$ cm. It has roll inertia of 1.94 E-2 kg-m^2, yaw inertia of 2.02 E-2 kg-m^2, and pitch inertia of 9.28 E-03 kg-m^2. The initial Euler angles ϕ, θ, and ψ and of the fin-stabilized system are 0, 3, and 0°, respectively. The fin-stabilized system is launched with a velocity of 350.52 m/s and a spin rate of 50 rad/s. The initial pitch and yaw rates and the side velocities are all equal to zero. The part roll rate control is initiated 0.5 s after the projectile is launched. It takes ~1 s to spin the part down to less than 1 rad/s and control the part to the desired roll orientation. The part is asymmetrically reformed 1.5 s into the flight. The maximum allowable control torque is set at 13.56 N-m. The commanded control angle ϕ_C is specified to be 0 rad for the trajectory of the nominal and modified two-body fin-stabilized systems. Both system trajectories are compared to that of an exemplary fin-stabilized rigid projectile. Included in the study are the trajectories of a fin-stabilized system that result if the axial drag of a modified two-body system projectile is increased by 30%.

Altitudes vs. range of the two-body systems are compared to that of a fin-stabilized rigid projectile in figure 6. The trajectory of the nominal system and the rigid projectile are coincident. All systems travel downrange and impact with a vertical target at a range of 3 km. The inertia of the modified system is such that it induces an increase in pitch at launch resulting in increased altitude. The modified drag system also experiences an initial increase in altitude, but this quickly reduces due to increased drag and results in a decrease in altitude at impact. In figure 7, cross range of the nominal two-body system is ~4 m greater than that of a rigid projectile in a direction opposite that of the part orientation. Cross range of the modified two-body system is ~27 m greater than that of a rigid projectile. Increasing axial drag of the two-body system by 30% further increases cross range over that of a rigid projectile to ~40 m. The forward velocity time histories of the fin-stabilized systems are compared to a rigid projectile in figure 8. The nominal system velocity is coincident with that of a rigid projectile, demonstrating that the inclusion of an internal part has little effect on the projectile forward velocity. The modified two-body system, however, flies at a slightly higher angle of attack, increasing drag, and noticeably reducing forward velocity. The roll rate time histories of a rigid projectile, the two-body systems, and their internal parts are shown in figure 9. The part roll rates are all coincident. Control of the part roll rate is not initiated until 0.5 s into the flight and a moment due to bearing friction causes roll rate of the part to decrease at a slower rate than that of the projectile body. When control is initiated at 0.5 s, torque is applied to the part, causing it to rotate in a direction opposite to that of the projectile. The applied torque acts on the projectile in an equal and opposite direction, causing it to spin down. Once control is implemented, it takes ~0.2 s to reduce roll rate of the part to less than 1 rad/s, and another 0.8 s to control the roll orientation of the symmetrical part to the desired angle relative to the nonrolling reference frame, as shown in figure 10. The maximum torque required to reduce the spin rate to less than 1 rad/s is ~0.30 N-m, as shown in figure 11. Once roll rate of the part is reduced, and reformed

asymmetrically at an offset from the projectile axis of symmetry, approximately half the maximum torque is necessary to control the disk at a specified angle. Angle of attack vs. time of the two-body systems is compared to that of a rigid projectile in figure 12. The inertial characteristics of the modified projectile cause an initial increase in the angle of attack of the modified two-body system at launch. Fixing the orientation of the mass unbalance and reforming the part asymmetrically (occurs at 1.5 s) perturbs the system dynamics affecting increases in the angle of attack of both two-body systems. It also induces lateral oscillations in the angle of attack, which decay over time. However, the perturbations due to the reformation of the part results in the modified two-body system angle of attack increasing with time. Fixing the orientation of the mass unbalance at a 0° control angle causes an increase in the Euler yaw angle of the two-body systems, as shown in figure 13. However, it has very little effect on Euler pitch angle shown in figure 14. If the part were fixed at an angle of 90 or 270°, a large increase would be seen in the Euler pitch angle and the Euler yaw angle would not be affected.

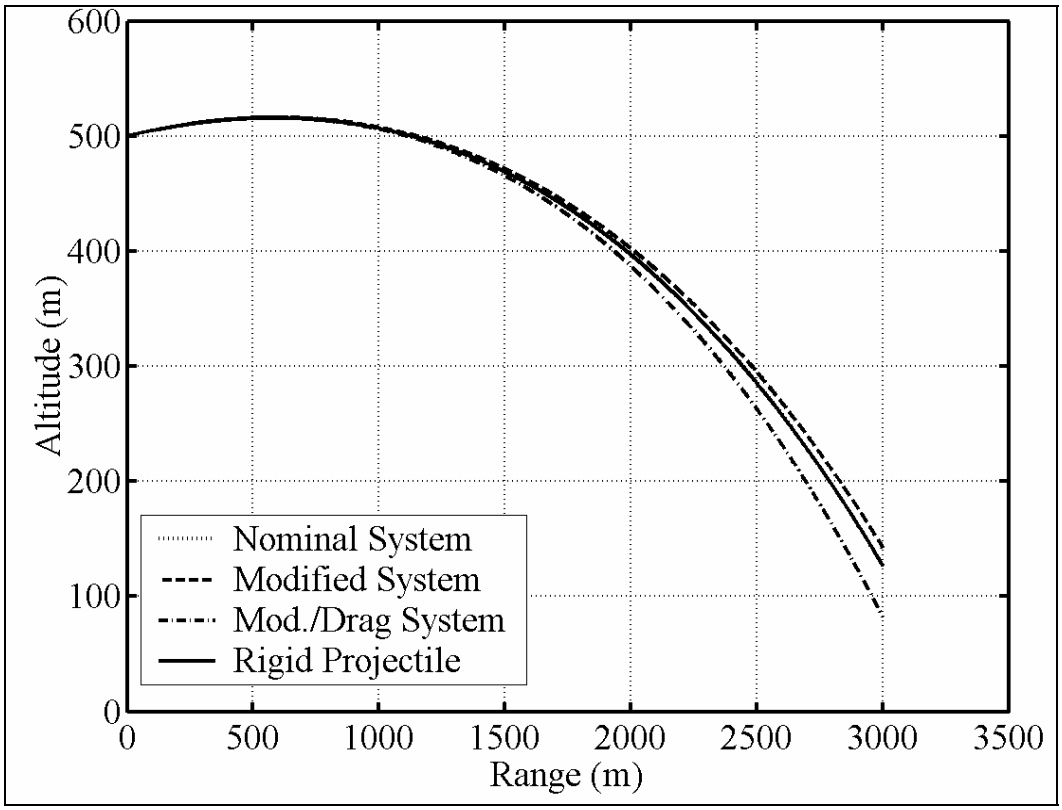

Figure 6. Fin-stabilized system altitude vs. range.

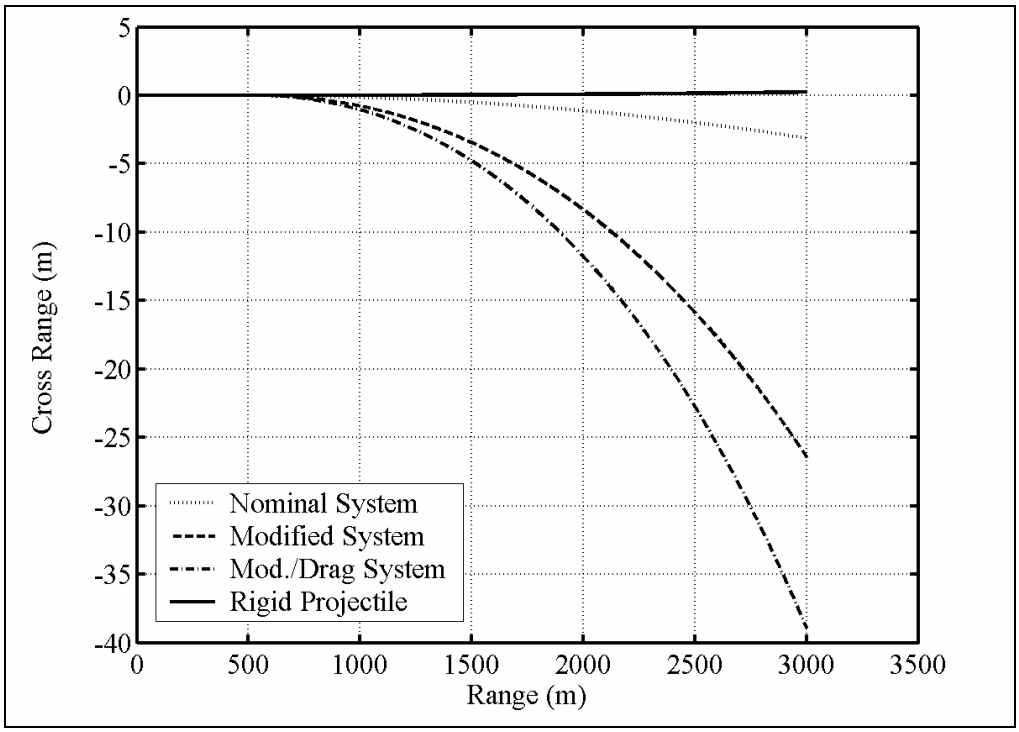

Figure 7. Fin-stabilized system cross range vs. range.

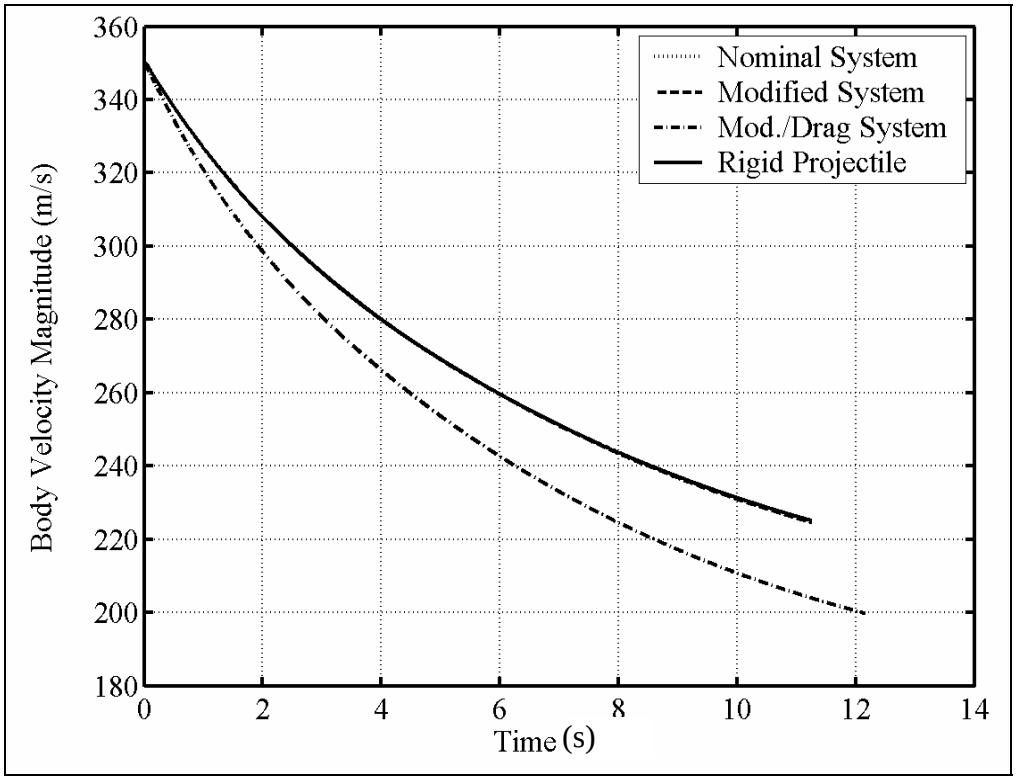

Figure 8. Fin-stabilized system magnitude of velocity time history.

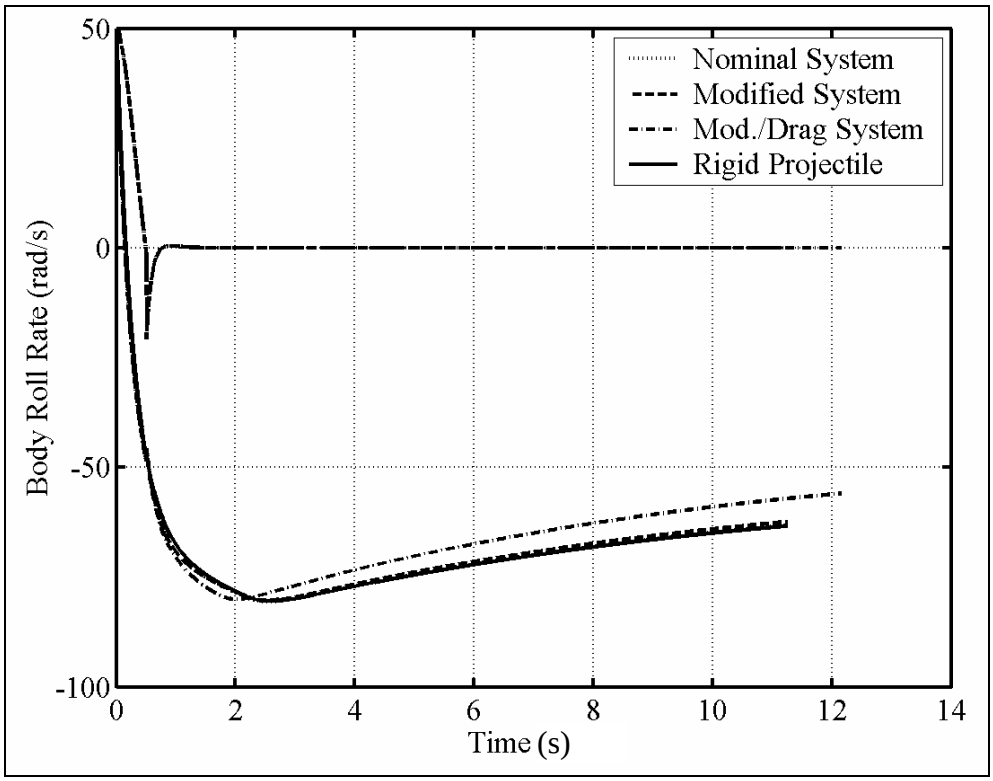

Figure 9. Fin-stabilized system roll rate time histories.

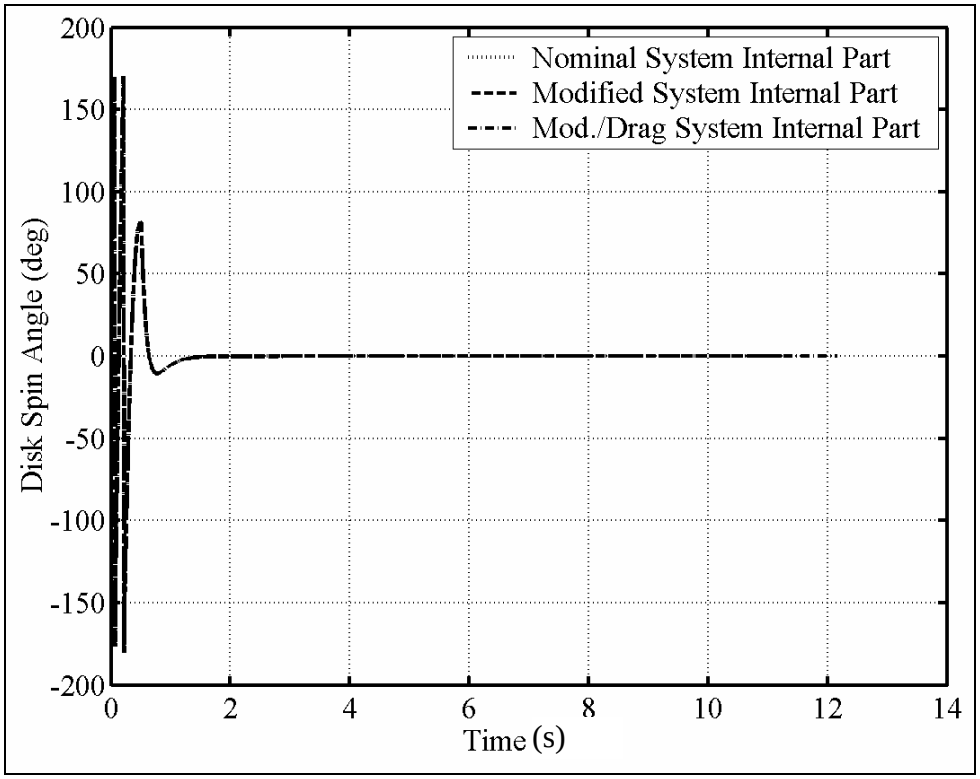

Figure 10. Fin-stabilized system part roll angle time histories.

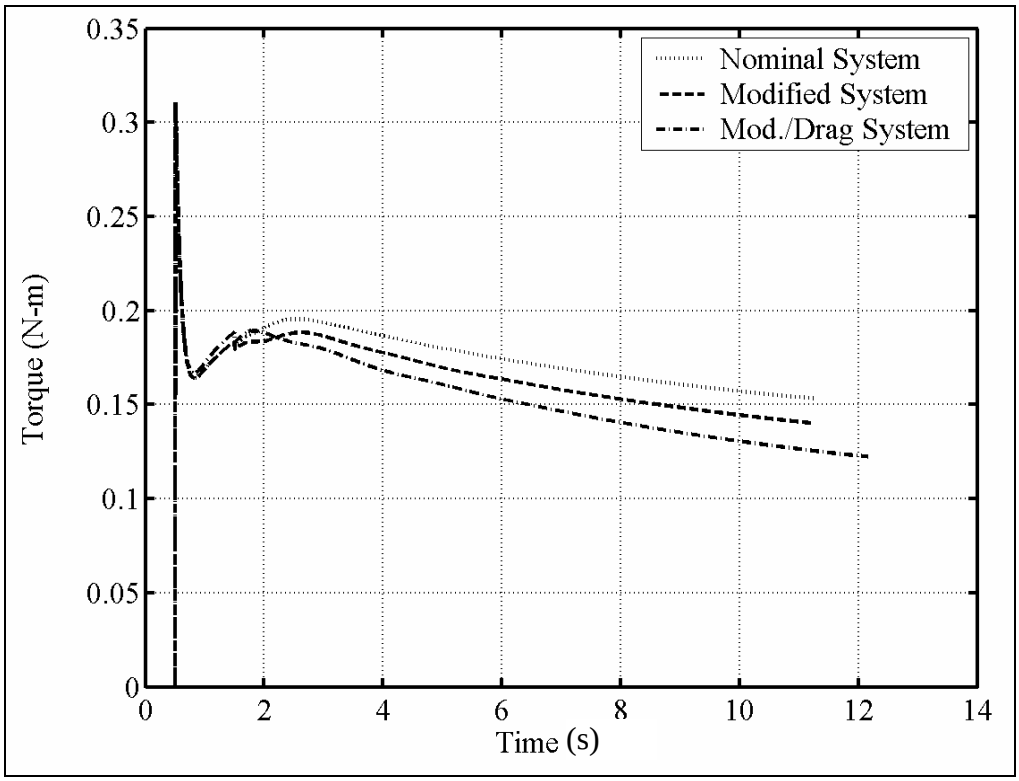

Figure 11. Fin-stabilized system control torque.

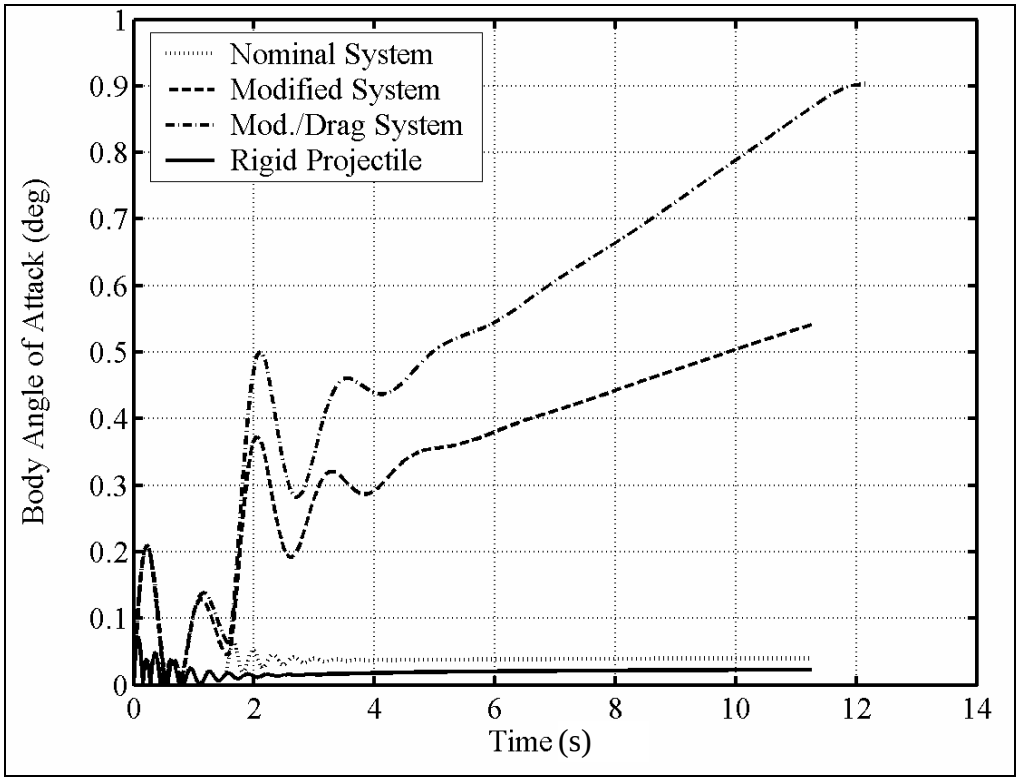

Figure 12. Fin-stabilized system angle of attack.

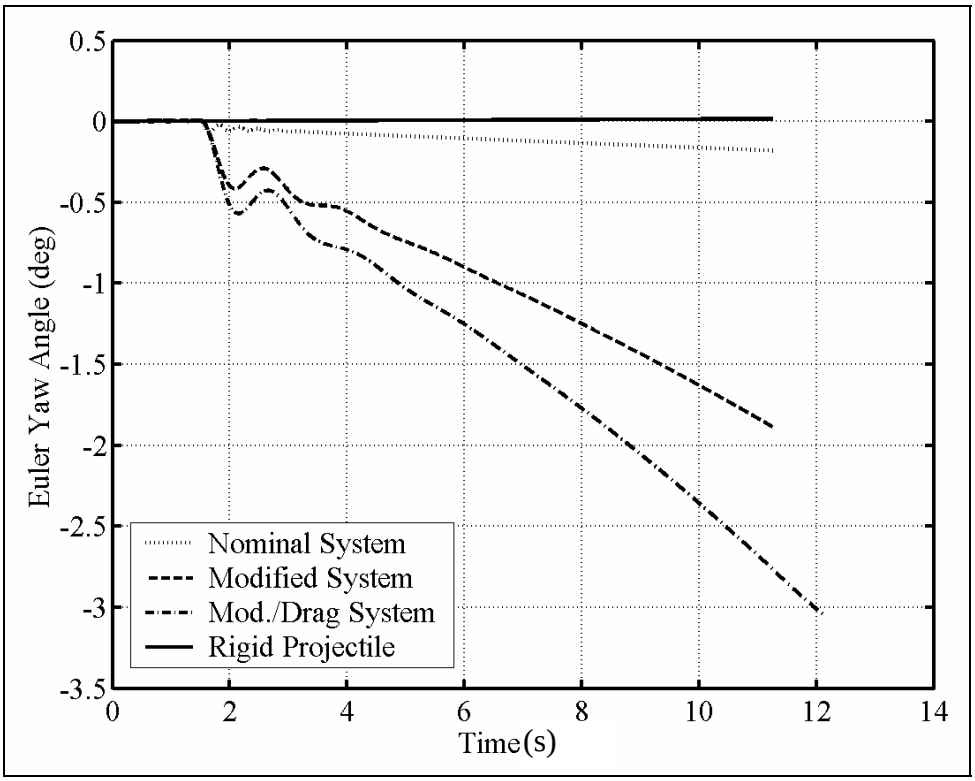

Figure 13. Fin-stabilized system Euler yaw angle.

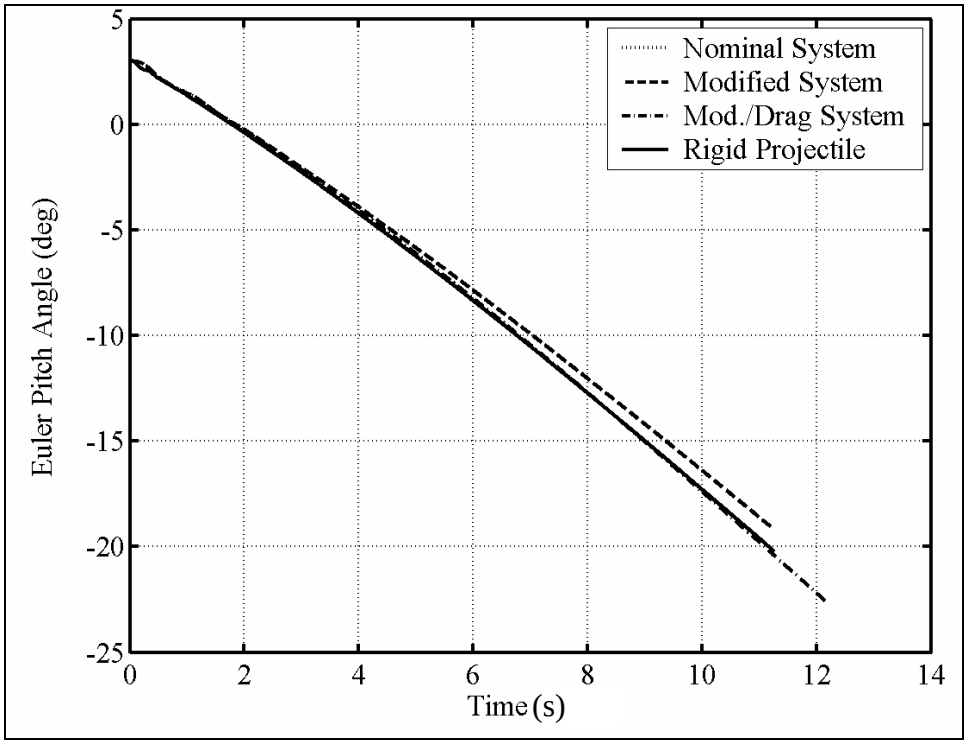

Figure 14. Fin-stabilized system Euler pitch angle.

In order to evaluate control authority size and shape, vertical plane dispersion patterns are shown in figure 15 for different part command angles. Control authority is defined as the dispersion pattern created by the set of impact points. Control authority is shown for the nominal and modified two-body systems and for the nominal and modified two-body systems with 30% increased axial drag. For this study, the orientation of the mass unbalance is controlled at angles from 0 to 360° in increments of 10°, and impact points are plotted with respect to the impact points of similar uncontrolled systems. Predictable dispersion patterns are achieved for given mass unbalance orientation angles. Moreover, increased control authority is achieved by modifying the mass, inertia, and aerodynamic properties of a rigid projectile such that it is fundamentally less stable than that of a typical fin-stabilized projectile.

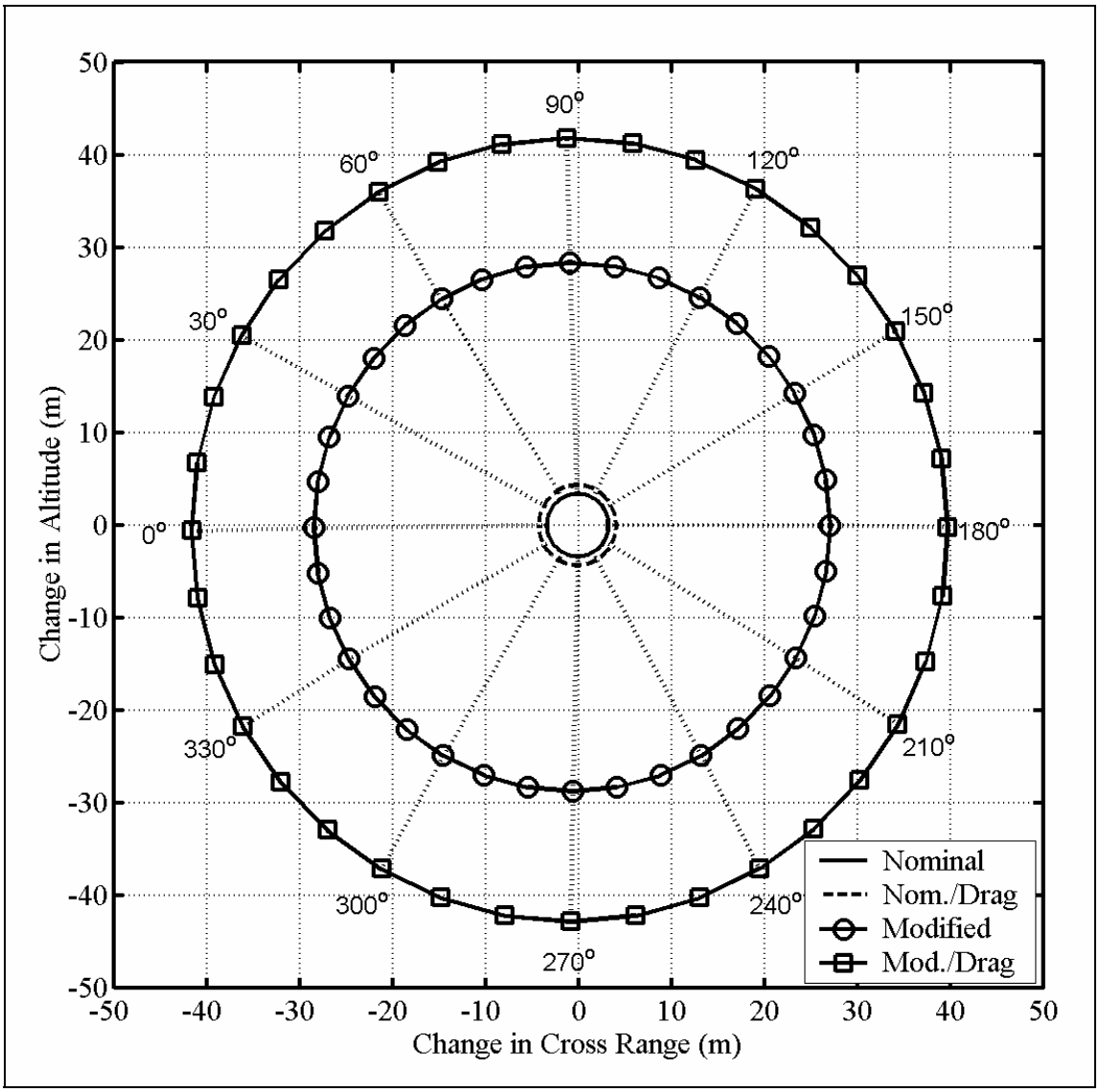

Figure 15. Control authority plot for fin-stabilized systems.

In order to evaluate the effect that velocity has on a system containing an internal part, dispersion patterns were generated for a range of launch velocities of a modified fin-stabilized system fired at a pitch angle of 3° from an altitude of 3000 m at a target 3000 m downrange. The effects of varying velocity are isolated from the time at which the internal mechanism is deployed by reforming the part asymmetrically at the same range (762 m) for each of the velocities. The radial mean of dispersion was calculated from the impact points generated by simulating the trajectories of the modified fin-stabilized system equipped with a semicylindrical part controlled at angles from 0 to 360° in increments of 10°. The radial mean of dispersion and average stationline distance from the center of pressure to the system center of gravity is plotted vs. average velocity in figure 16. The increase in control authority at lower velocities is due to the fact that fin-stabilized systems usually become less stable at lower velocities, and therefore perturbation due to the axial drag induced moment results in a greater increase in yaw and consequently dispersion. The decrease in stability is a result of the Mach number dependent stationline center of pressure approaching the system stationline center of gravity at lower velocity. This observable fact is shown in figure 16, where average stationline distance from the center of pressure to the system stationline center of mass is plotted vs. velocity on the right-hand side of the graph. Consequences of increasing dispersion by lowering velocity are an increase in time to target and a loss in altitude, as shown in figures 17 and 18.

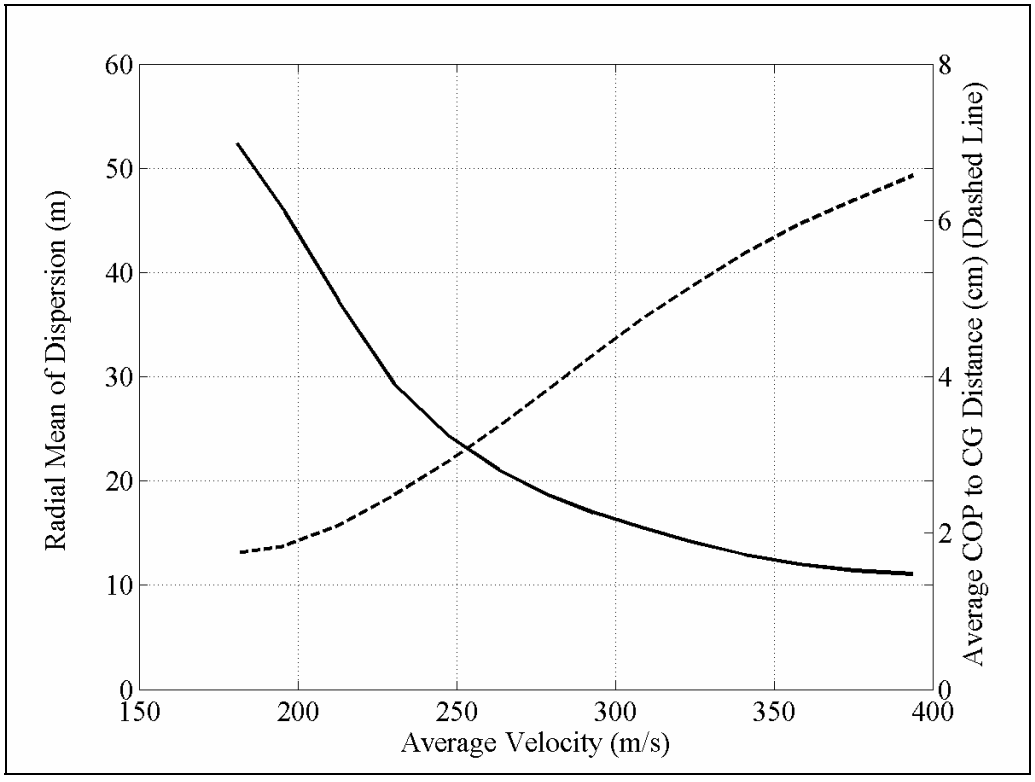

Figure 16. Fin-stabilized dispersion and average stationline distance vs. average velocity.

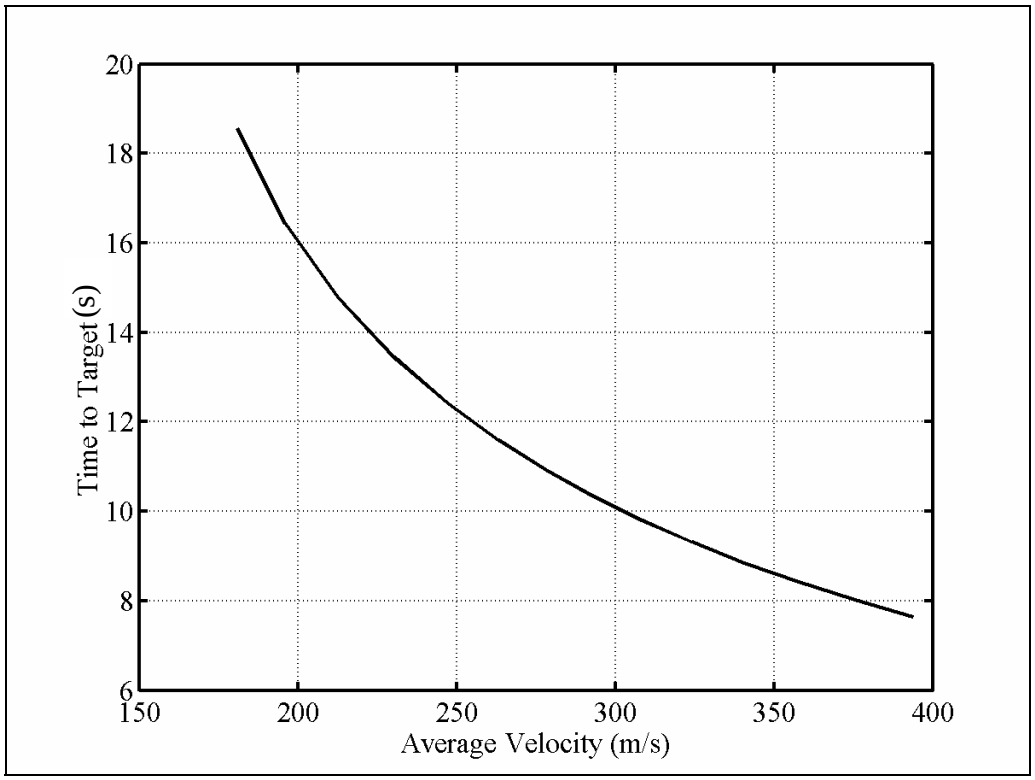

Figure 17. Fin-stabilized system time to target as a function of velocity.

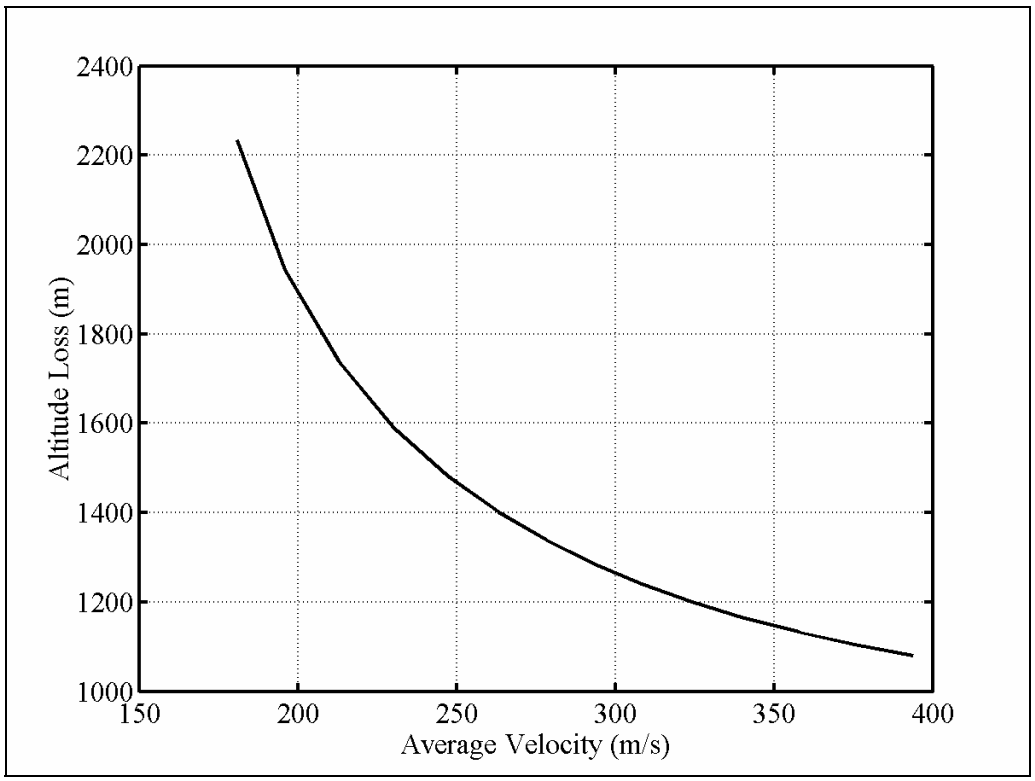

Figure 18. Fin-stabilized system loss in altitude as a function of velocity.

A subsequent study was performed to determine the effects of using an internal part as a control mechanism for a spin-stabilized projectile. The flight characteristics of a nominal, modified, and drag modified spin-stabilized system were simulated and compared to the flight characteristics of a nominal and modified rigid spin-stabilized projectile. Results are shown for a typical 155-mm spin-stabilized artillery shell having a nominal weight of 422 N. The nominal stationline, buttline, and waterline distances to the nominal spin-stabilized projectile center of mass are 0.32, 0, and 0 m, respectively, measured from the base. The stationline, buttline, and waterline distances to the modified projectile center of mass are 0.62, 0, and 0 m, respectively, measured from the base. The spin-stabilized projectile nominal roll inertia is 0.48 kg-m^2, and the nominal pitch and yaw inertias are 6.21 kg-m^2. The spin-stabilized projectile modified roll inertia is 0.61 kg-m^2, and the modified pitch and yaw inertias are 5.35 kg-m^2. The reformed internal part contained in the spin-stabilized system consists of a semicylindrical shaped lead part that has a mass of 4.58 kg, a radius of 6.35 cm, and is 6.35 cm thick. The part-to-projectile connection point is located at the composite body center of mass. When reformed asymmetrically, the part center of mass is radially offset from the projectile axis of symmetry a distance of $\varepsilon = 2.69$ cm. It has a roll inertia of 1.94 E-2 kg-m^2, a yaw inertia of 2.02 E-2 kg-m^2, and a pitch inertia of 9.28 E-03 kg-m^2.

The initial Euler angles ϕ, θ, and ψ of the spin-stabilized projectile are 0, 30, and 0°, respectively. The spin-stabilized projectile leaves the muzzle with a velocity of 838.20 m/s and a spin rate of 1675 rad/s. The initial pitch and yaw rates and the side velocities are all equal to zero. Part roll rate control is initiated 2 s after the projectile leaves the muzzle. It requires ~3 s to spin the part down to less than 1 rad/s and another 0.5 s to control the part to the desired roll orientation. The part is asymmetrically reformed 6 s into flight. The maximum allowable control torque is 13.56 N-m. The commanded control angle ϕ_C is specified to be 0°. In order to determine the effects altering the aerodynamics of a modified projectile have on a spin-stabilized system, the Mach number dependent, drag, and lift force coefficients of the modified spin-stabilized projectile are increased by 30%. However, indirect fire weapons suffer a loss in range and altitude with increased drag; therefore, the increased control authority due to the moment produced from axial drag about the system center of mass is offset by the loss in time of flight. In order to compare the effects of altering drag and lift coefficients on the system, the muzzle velocity of the modified drag system is increased to 960 m/s to compensate for the loss in altitude and range caused by the increase.

Altitude vs. range of nominal, modified, and modified drag, two-body systems is compared to that of nominal and modified rigid projectiles in figure 19. The inertia of the modified two-body system is such that it induces a negative pitch rate at launch. Because of gyroscopic effects inherent in spinning projectiles, the negative pitch rate results in a positive increase in altitude and consequent increase in range. Increasing the axial and normal drag by 30% of the modified drag system and increasing its muzzle velocity to 960 m/s increases the altitude while maintaining approximately the same range as the modified system. A further increase in altitude

is gained by the two-body systems over the altitude of the rigid projectiles because of increased spin rate due to the axial torque necessary to orient the internal part. Figure 20 shows that controlling the internal part at an angle of 0° results in an increased range of ~20 m over that of a nominal rigid projectile. It affects an increase in cross range of ~55 m over that of an uncontrolled two-body system in the direction of the part orientation. Controlling the internal part at an angle of 0° in a modified two-body system results in an increased range of ~80 m and an increased cross range of ~90 m over that of a modified rigid projectile. Increasing the drag and lift coefficients further increases the cross range to ~190 m; however, range is decreased by ~55 m. Note that the spin-stabilized system lateral swerve in the horizontal plane is in a direction opposite to that of the motion that would be intuitively produced as a result of the axial drag acting about the composite body center of gravity. Referring to figure 7, it can be seen that the direction of horizontal plane swerve for a fin-stabilized system is opposite that of a spin-stabilized system for the same part orientation control angle. The forward velocity time histories of the nominal and modified two-body systems that are compared in figure 21 are almost coincident, demonstrating that the inclusion of an internal part has little effect on a spin-stabilized system's forward velocity. The modified two-body system, however, flies at a slightly higher angle of attack, increasing drag, and slightly reducing the forward velocity (~3 m/s).

The modified drag system reduction in forward velocity is due to the increased axial force. The roll rate time histories of the controlled two-body systems and their internal parts are shown in figure 22. Control of the part roll rate is not initiated until 2 s into the flight and a moment due to bearing friction causes roll rate of the part to decrease at a reduced rate than that of the projectile body. When control is initiated at 2 s, torque is applied to the part causing it to rotate in a direction opposite to that of the projectile. The applied torque acts on the projectile in an equal and opposite direction, causing it to spin up. The modified systems have greater roll inertia than the nominal system, and do not spin up as quickly or to as large a rate. However, because of the greater roll inertia, the modified systems' spin rates are not damped out to the same extent as the nominal system's spin rate. Once control is implemented, it requires ~3 s to reduce roll rate of the part to less than 1 rad/s, and another 0.5 s to control the roll orientation to the desired angle relative to the nonrolling reference frame (figure 23). In order to achieve zero spin rate with respect to the no-roll frame, the part is spun at a rate equal and opposite to that of the projectile. For a spin-stabilized system, this initially requires a significant torque and during this time the controller is saturated as shown in the control torque profile in figure 24. Once roll rate of the part is reduced, and reformed asymmetrically at an offset from the projectile axis of symmetry, the torque necessary to control the disk at a specified angle becomes more manageable and changes in angle can be achieved in less than 0.5 s. Angle of attack vs. time of the controlled two-body systems is compared to that of the rigid projectiles in figure 25. Inertial characteristics of the modified projectile cause an initial increase in the angle of attack of the modified two-body system at launch. Fixing the orientation of the mass unbalance (which occurs at 6 s) perturbs the system dynamics affecting increases in the angle of attack of the controlled two-

body systems. It also induces lateral oscillations of the nominal two-body system angle of attack, which decay over time. Fixing the mass unbalance at an angle of 0° in the controlled systems increases their Euler yaw and pitch angles, as shown in figures 26 and 27. A greater increase in these angles is achieved in the modified systems.

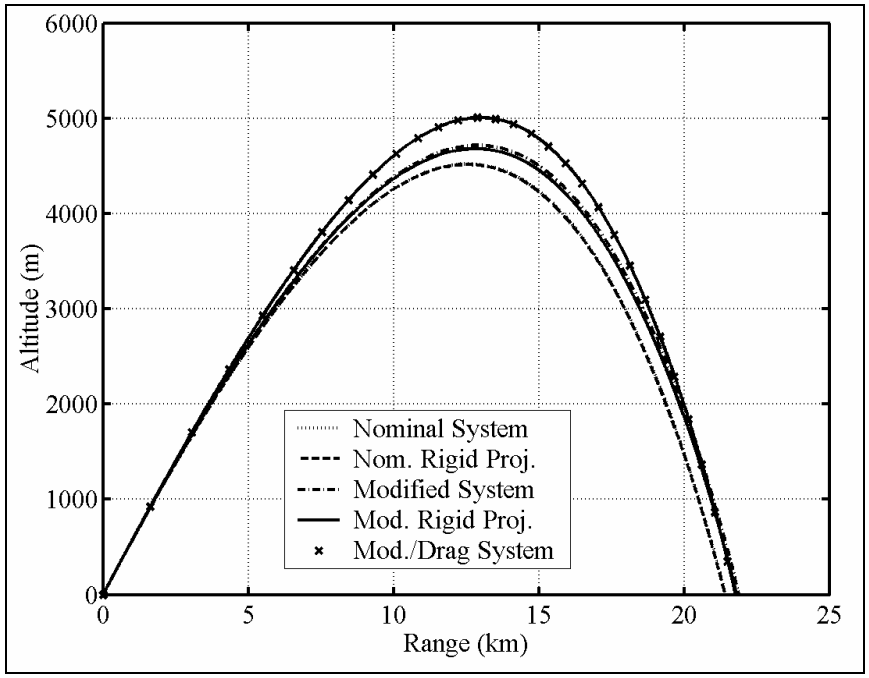

Figure 19. Spin-stabilized system altitude vs. range.

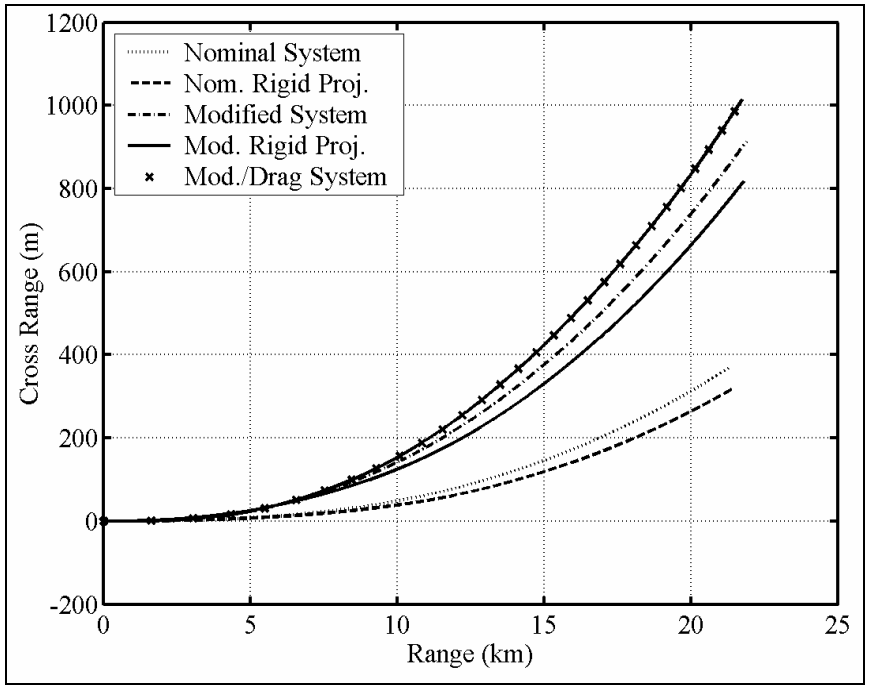

Figure 20. Spin-stabilized system cross range vs. range.

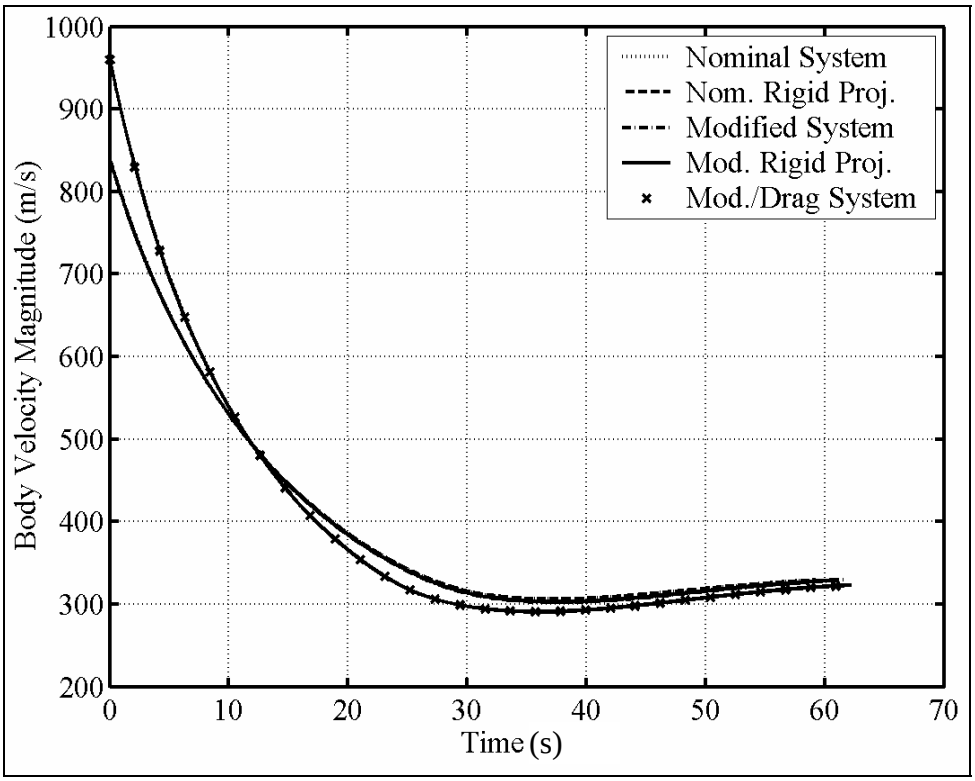

Figure 21. Spin-stabilized system magnitude of velocity time history.

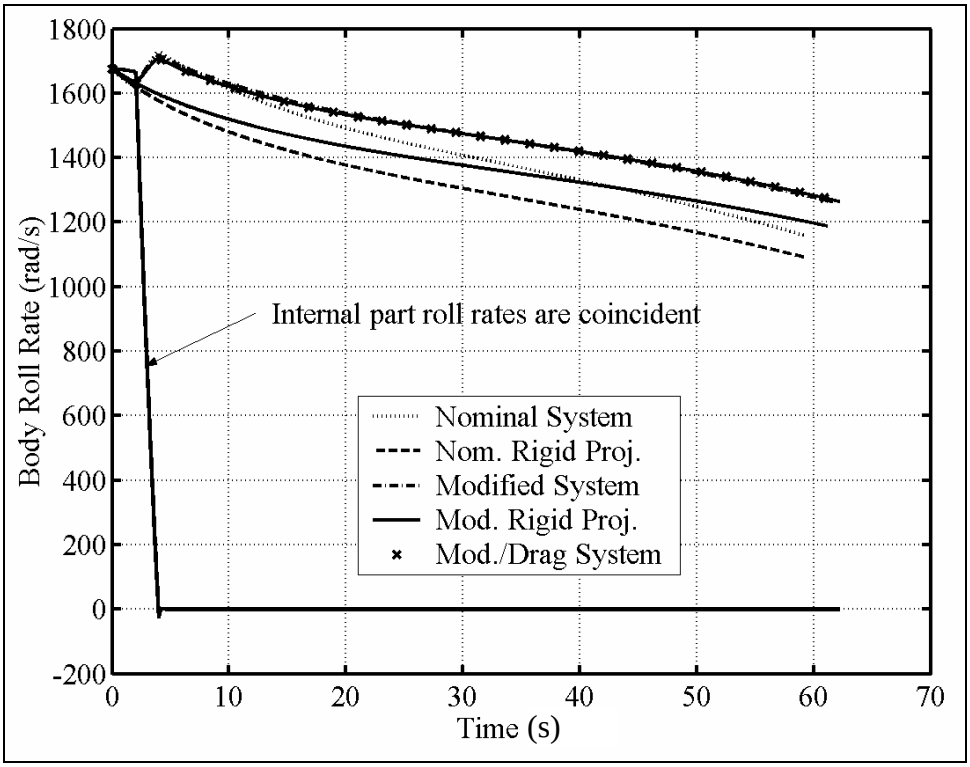

Figure 22. Spin-stabilized system roll rate time histories.

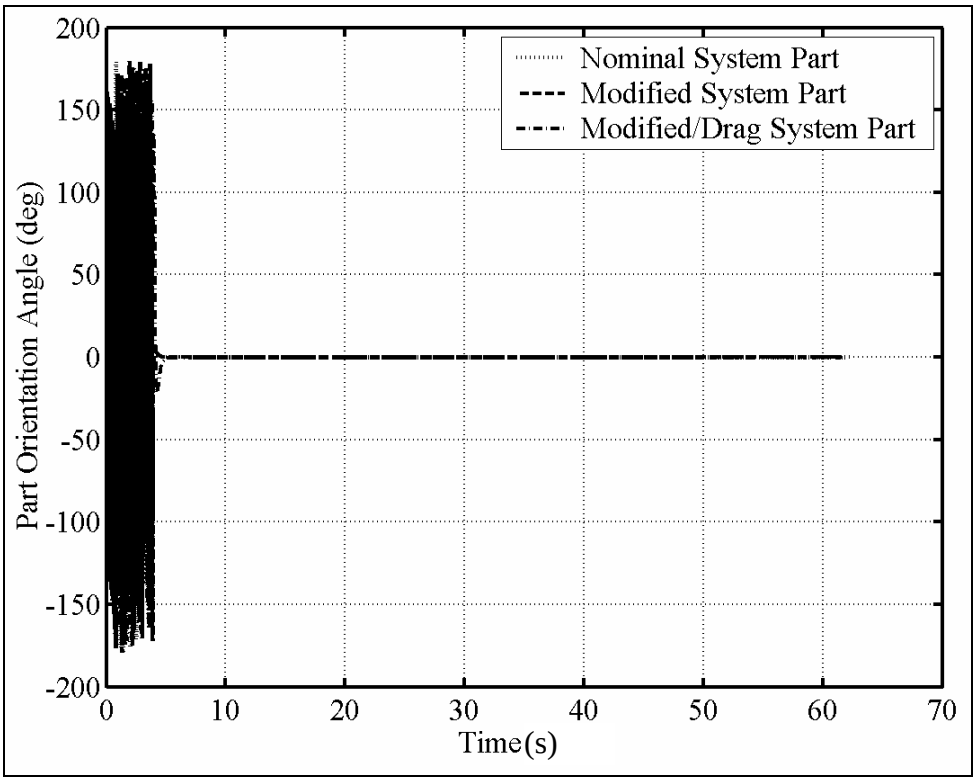

Figure 23. Spin-stabilized system part orientation angle time history.

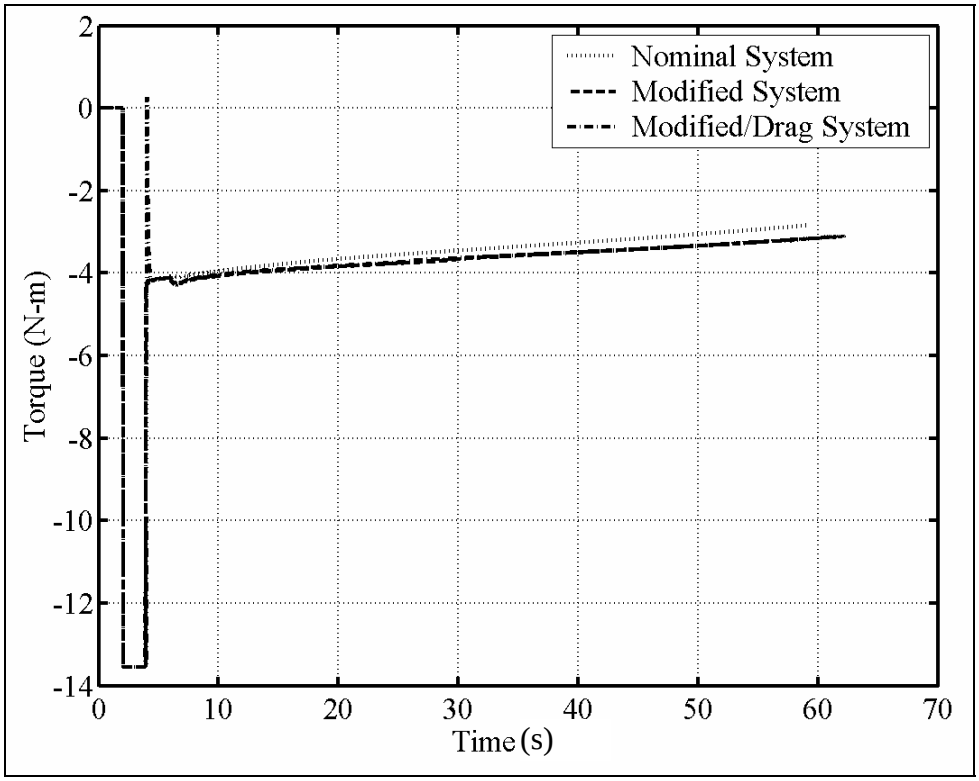

Figure 24. Spin-stabilized system control torque.

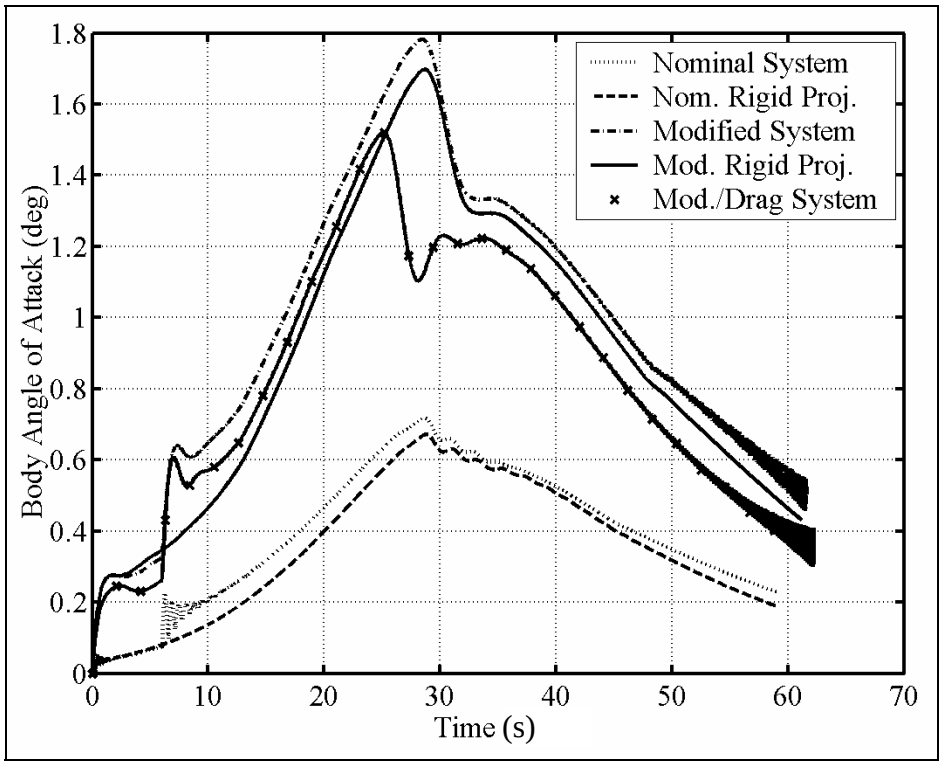

Figure 25. Spin-stabilized system angle of attack.

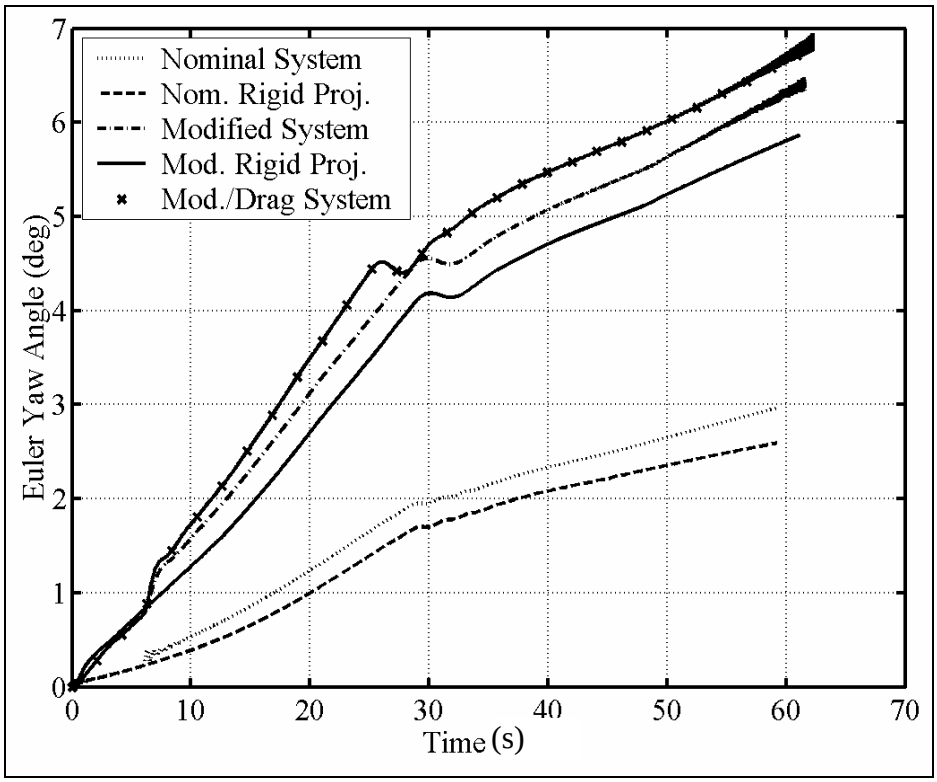

Figure 26. Spin-stabilized system Euler yaw angle.

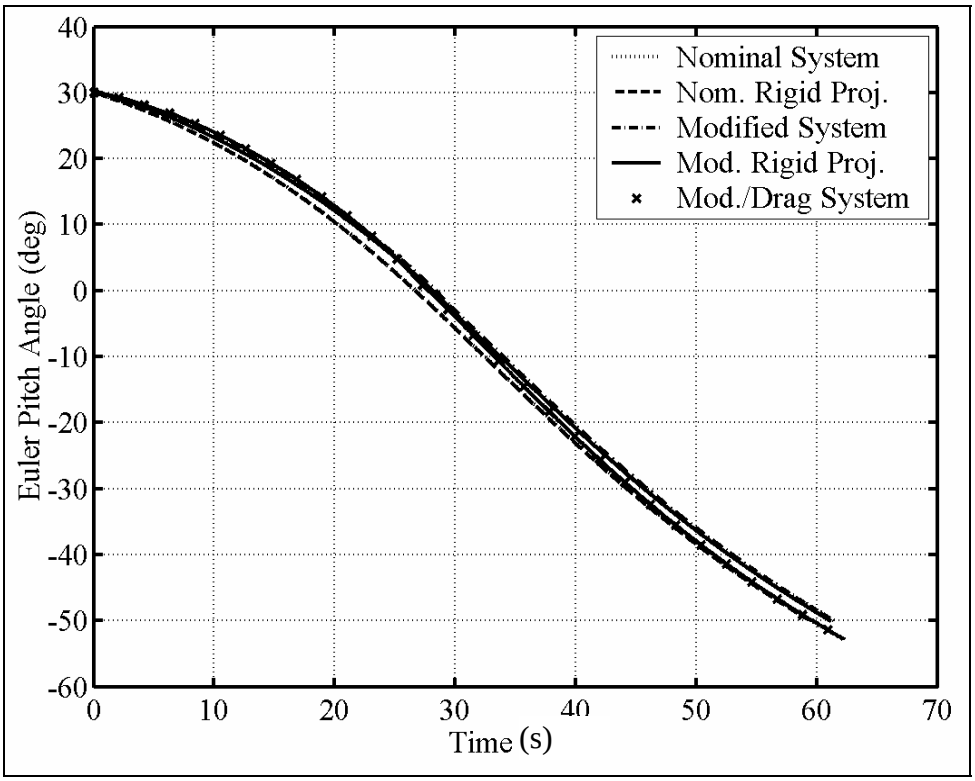

Figure 27. Spin-stabilized system Euler pitch angle.

In order to evaluate the effect that controlling the orientation of the mass unbalance at different angles has on a spin-stabilized system, dispersion patterns shown in figure 28 are generated for the nominal, modified, and modified drag, two-body spin-stabilized systems. As in the fin-stabilized study, the orientation of the mass unbalance is controlled at angles from 0 to 360° in increments of 10°. Ground impact points are plotted with respect to the impact points of a similar rigid projectile. The patterns are laterally shifted about the rigid projectile impact points because of the increased roll rates of the controlled systems. These axial torque induced roll rates produce Magnus forces that cause the controlled systems to swerve more laterally. Figure 28 is significant in the fact that it shows that predictable dispersion patterns are achieved for given mass unbalance orientation angles for a spin-stabilized system as well as for a fin-stabilized system. Increased control authority is also achieved with a spin-stabilized system by modifying the inertia and aerodynamic properties of the nominal rigid projectile such that it is fundamentally less stable then that of a typical spin-stabilized projectile. Altering the aerodynamic properties changes the dynamics of the system such that the impact points for given angles are out of phase with the impact points generated from the same angles of a nonaerodynamically altered system.

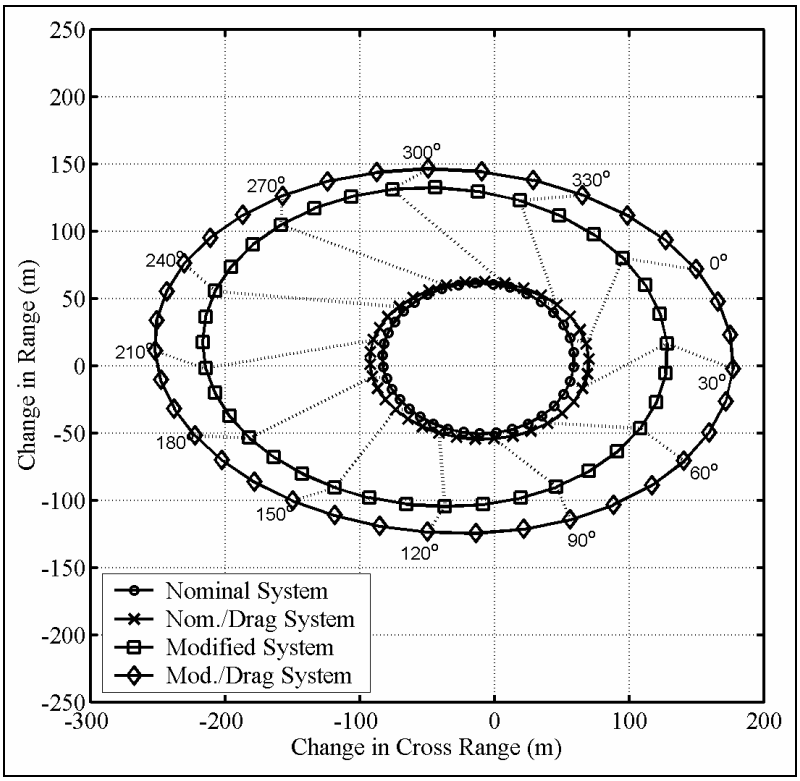

Figure 28. Control authority plot for spin-stabilized systems fired at Q.E. = 30°.

Figure 29 shows the dispersion patterns for a nominal spin-stabilized system fired at quadrant elevations of 15, 30, and 45°. Range control of an internal part control mechanism is limited in indirect fire weapons by the angle of fire. Changes in cross range are proportional to the quadrant elevation of the muzzle; however, changes in range are sensitive to the pitch angle of the projectile. To demonstrate this phenomenon, the system was fired at several different quadrant elevations, and the effected change in range is plotted vs. the change in pitch angle shown in figure 30. For a system fired at a quadrant elevation of 50°, any change in pitch angle affected by the internal mechanism produces very little change in range.

A modified spin-stabilized system was fired at a quadrant elevation of 30° with a semicylindrical internal part controlled at angles from 0 to 360° in increments of 10° and reformed asymmetrically 6 s into the flight. Muzzle velocity was varied from 595 to 1265 m/s. The initial roll rate was assumed constant and all other initial conditions were as given in the trajectory study previously discussed. In order to isolate the effects of velocity on the trajectory, the radial mean of dispersion per trajectory length is plotted vs. average velocity in figure 31. Unlike a fin-stabilized system, spin-stabilized systems achieve greater control authority with higher velocity. In a spin-stabilized system, the Mach number dependent stationline center of pressure shifts aft toward the system stationline center of gravity as velocity is increased, thus destabilizing the system. This finding is shown in figure 31 where average stationline distance from the center

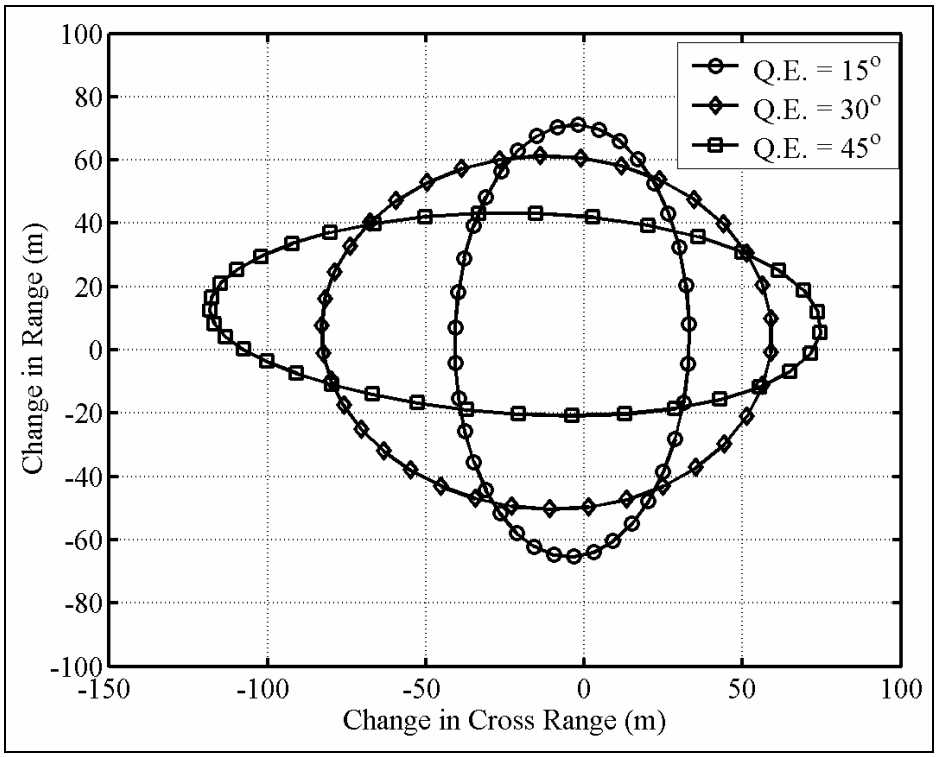

Figure 29. Control authority plots for a nominal spin-stabilized system (Q.E. = 15, 30, and 45°).

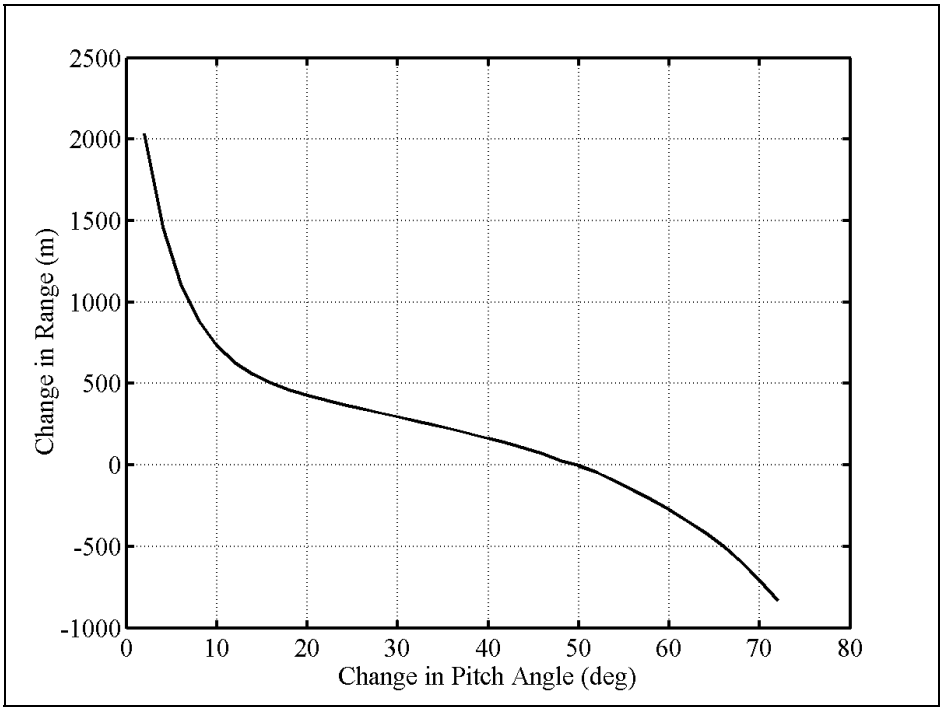

Figure 30. Pitch angle sensitivity.

of pressure to the system center of mass is plotted on the right hand side of the graph. This destabilization allows the perturbations due to axial drag-induced moments to have a greater impact on the amount of control authority.

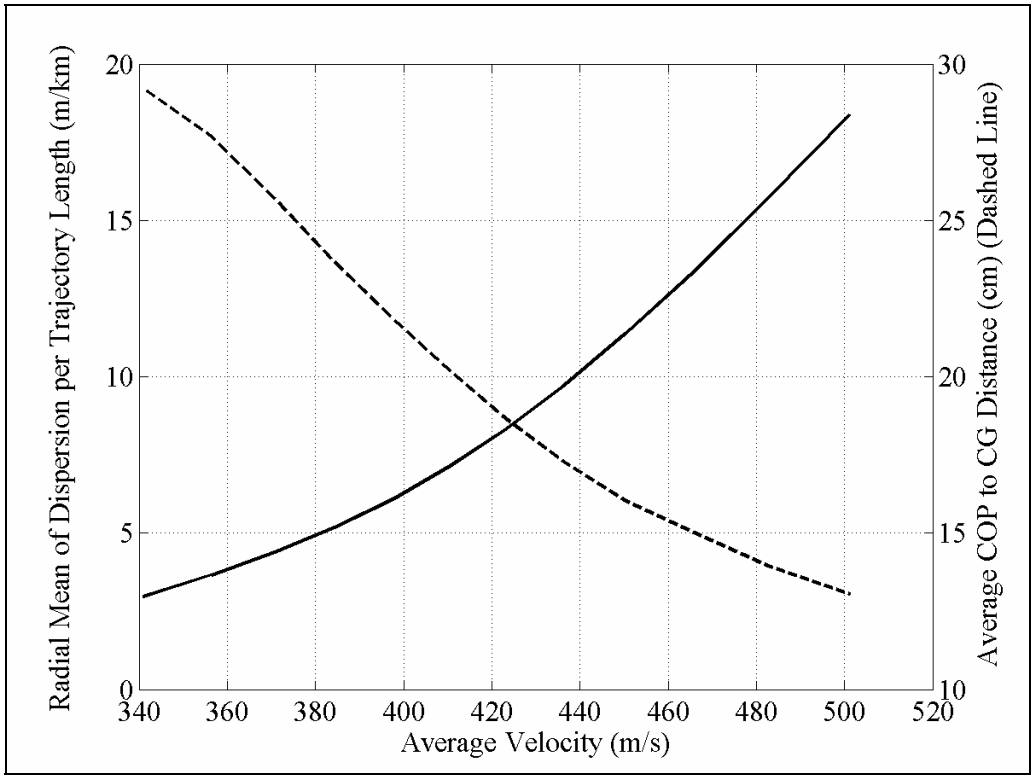

Figure 31. Spin-stabilized dispersion and average stationline distance vs. average velocity.

The effect of increasing part mass or increasing the distance the part center of mass is offset from the projectile axis of symmetry acts to increase control authority. However, the size and shape of the part is constrained by the size and shape of the projectile that it is contained within. A study was conducted in which material was removed in increasing radial amounts (as shown in figure 32) from a disk shaped part contained in a modified fin-stabilized system. Removing material from the disk results in a trade-off between increased mass center offset distance and decreased part mass. The radial mean of dispersion was calculated from the impact points generated by simulating the trajectories of a modified fin-stabilized system equipped with the various parts controlled at angles from 0 to 360° in increments of 10°. By generating the dispersion patterns and calculating the radial mean, it is shown in figure 33 that control authority is linearly proportional to the mass of the part times the radial offset of the part center of mass. The radial mean produced by the most mass and smallest offset distance is recorded at the bottom left of the curve. As mass decreases and offset distance increases, the curve slopes up and to the right. As mass decreases further, the curve retraces itself back to the bottom left. The same study conducted for a spin-stabilized system produces an identical trend. The largest radial mean is achieved using a semicylindrical part, as depicted in figure 3, with $\mu = 0$.

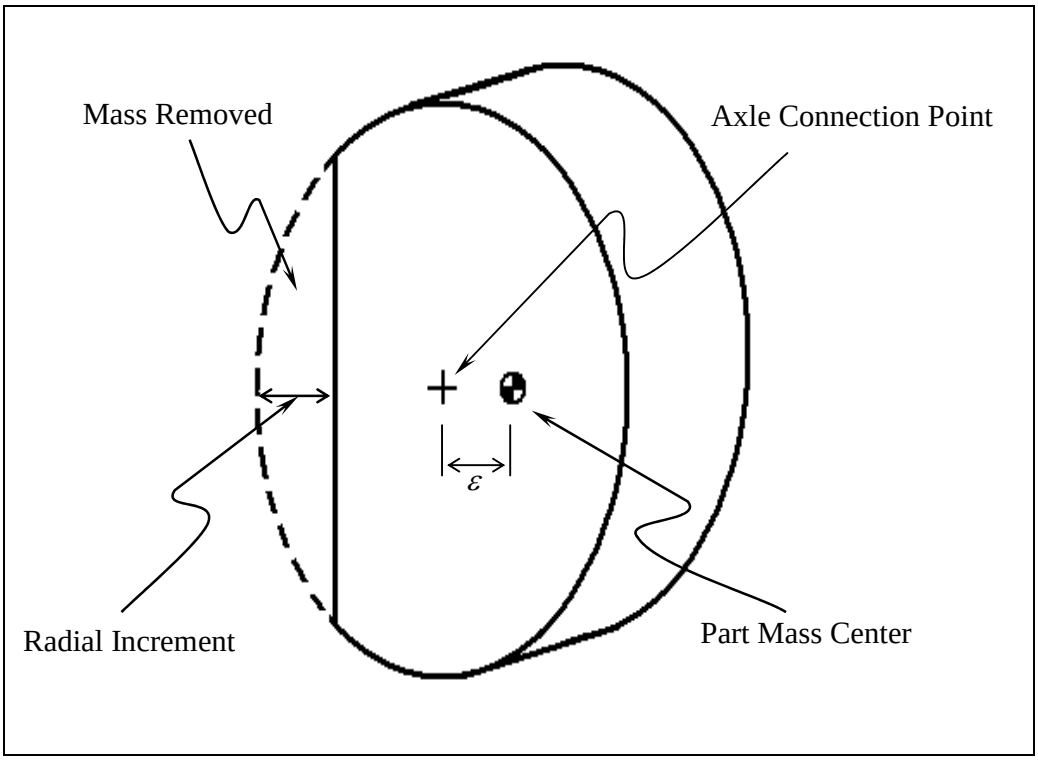

Figure 32. Part mass removal configuration.

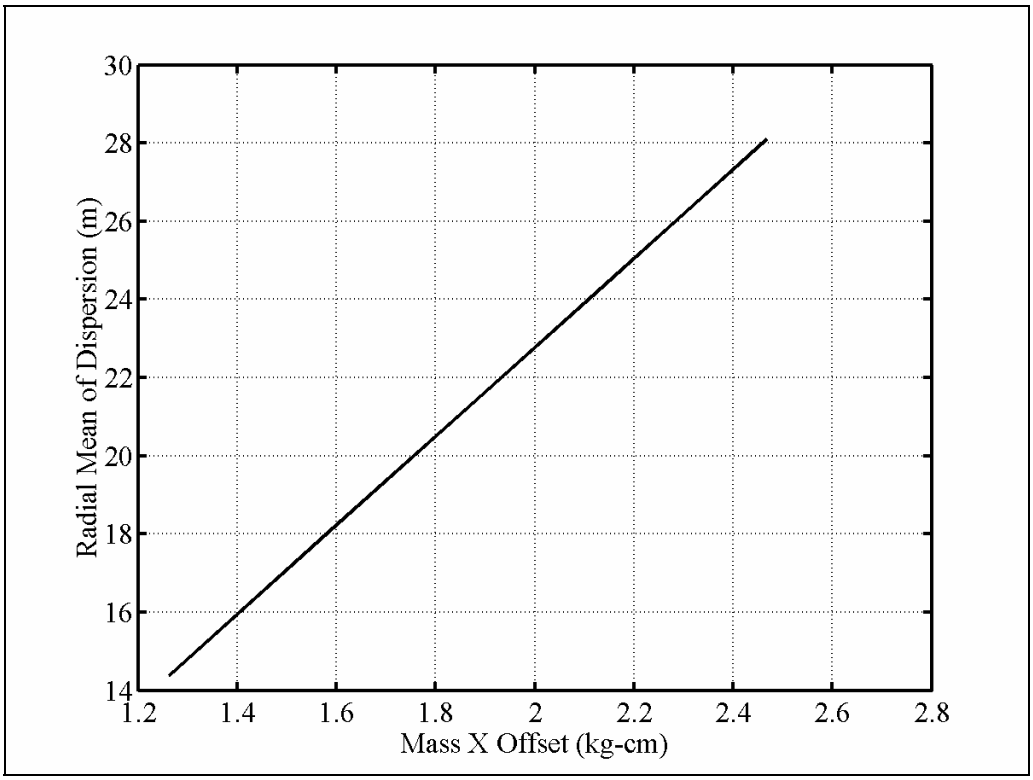

Figure 33. Dispersion as a function of part mass times part mass center offset.

In order to evaluate the effect that mechanism activation time has on control authority, dispersion patterns are shown for a modified spin-stabilized system fired at a quadrant elevation of 30° with nominal initial conditions. The allowable control torque was specified to be unlimited and the reformation time of the part was varied. The resulting radial mean of dispersion is plotted vs. the part reformation time in figure 34. For an ideal system in which control torque is unlimited and the part is considered controlled at the desired orientation at firing, control authority achieved is greatly increased to a value of ~380 m. The amount of dispersion is greatly reduced as the time of part reformation is increased.

Figure 34. Spin-stabilized dispersion vs. time of part reformation.

Typical dispersion results for an uncontrolled nominal fin-stabilized rigid projectile based on a sample of 200 trajectories subjected to initial and in-flight errors are shown in figure 35. Induced launch errors are normally distributed random variables with means equal to zero. The standard deviations are as follows: launch range position and launch cross range position standard deviations = 6.56 m, launch elevation aiming error = 0.34°, launch azimuth aiming error standard deviation = 0.23°, forward velocity error standard deviation = 13.12 m, pitch and yaw rate error standard deviation = 0.3 rad/s, side velocity errors standard deviations = 6.56 m/s, and mean wind magnitude standard deviation = 6.56 m/s. The mean wind direction is considered as a uniformly distributed random variable varying from 0 to 360°. The circular error probable (CEP) shown as a dotted line in figure 35 is defined as the minimum radius of a circle centered at the mean impact point and containing at least 50% of the shot impact points (shown as x's). The

control authorities for nominal, modified, and modified drag fin-stabilized systems are shown on figure 35 as solid lines and are labeled accordingly. Ideally, a practical control mechanism has control authority significantly greater than the CEP of the uncontrolled round. However, impact point dispersion can only be reduced to the accuracy of a weapon's position estimate in the vicinity of the target and the control authority suggested from the simulation should be tempered against position estimate errors that add to dispersion characteristics of a fielded weapon. The dispersion generated from the trajectories of a nominal fin-stabilized rigid projectile subjected to errors induced at launch and in flight result in a CEP of 27.4 m. The CEP shown in figure 35 is almost coincident with the control authority of the modified fin-stabilized system; however, the control authority plot is slightly elliptical and the CEP circle is barely visible just inside it. The control authority for a controlled nominal system contains only 1.5% of all impact points produced from errors induced at launch and during flight. This result establishes the fact that an internal part control mechanism is not a viable system for decreasing dispersion of the nominal system. However, the modified and modified drag system yield control authority that contains 48.5% and 79.5% of all impact points generated. This indicates that a controlled modified fin-stabilized system is capable of creating impact point changes that are the same order of magnitude as 50% of those caused by errors induced at launch and in flight. A controlled modified drag fin-stabilized system is capable of creating impact point changes that are the same order of magnitude as roughly 80% of all error induced dispersion.

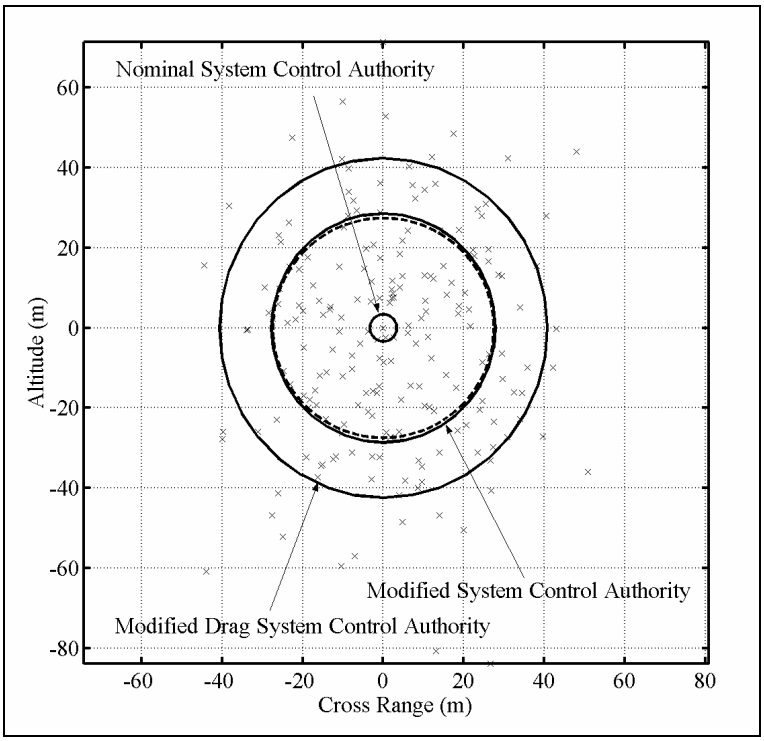

Figure 35. Uncontrolled dispersion of a fin-stabilized rigid projectile and fin-stabilized system control authority.

Typical dispersion results based on a sample of 200 trajectories subjected to initial and in-flight errors for an uncontrolled nominal spin-stabilized rigid projectile fired at a 30° quadrant elevation are shown in figure 36. The induced errors are the same as those for the fin-stabilized systems except for initial pitch and yaw rate, which have specified means of 0 rad/s and standard deviations of 2 rad/s. The labeled solid lines shown in figure 36 are the control authorities for nominal, modified, and modified drag spin-stabilized systems. A CEP of 165 m is obtained for the uncontrolled nominal system. A controlled nominal spin-stabilized system is only capable of a control authority that contains 11.5% of all impact points generated, and a controlled modified spin-stabilized system has control authority that contains 37.5% of all impact points generated. A modified drag spin-stabilized system equipped with an internal part control mechanism creates impact point changes that are the same order of magnitude as 50.5% of those caused by errors induced at launch and in flight.

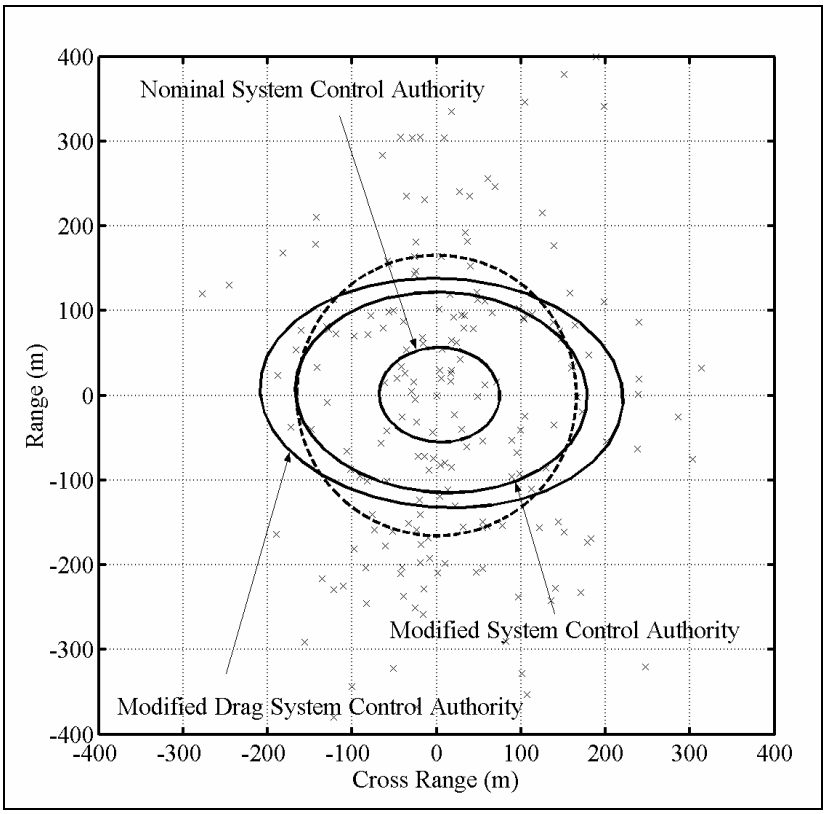

Figure 36. Uncontrolled dispersion of a spin-stabilized rigid projectile and fin-stabilized system control authority.

8. Conclusions

A seven DOF flight dynamic model is documented and subsequently used for trajectory predictions of fin-stabilized and spin-stabilized projectiles equipped with internal unbalanced

rotating parts. It is shown that holding the unbalanced part in a fixed roll orientation with respect to the no-roll reference frame causes predictable trajectory changes with respect to an uncontrolled system including predictable impact point changes. The main mechanism for steering the projectile is a moment produced by axial drag about the composite body center of mass that is created by positioning the part in a fixed roll orientation. Control authority for both types of systems is shown to increase proportionally as the multiplicative value of unbalance-offset distance times part mass is increased. The amount of control authority achieved is greatly increased the earlier in flight that control is initiated. Fin-stabilized system control authority is increased with lower average flight velocity, while spin-stabilized system control authority is increased with higher average flight velocity. The effect of decreasing or increasing the velocity in the appropriate system is to destabilize the projectile by moving the center of pressure closer to the center of gravity such that it is more responsive to perturbations caused by axial drag induced moments. It should be noted that range control of an internal part control mechanism is limited in indirect fire weapons by the angle of fire. Changes in cross range are proportional to the quadrant elevation of the muzzle; however, changes in range are sensitive to the pitch angle of the projectile. Internal part control mechanisms do not effect sizeable reductions in dispersion when employed in standard weapon systems. In order to achieve significant reductions in dispersion, internal part control mechanisms must be coupled with systems that are fundamentally less stable than current standard off-the-shelf weapons.

9. References

1. Richardson, D. Summoning the Fire. *Armada International* **2003**, *27*, 10.
2. Gander, T. J. Artillery O Target—Trajectory Correctable Munitions. *Armada International* **2003**, *27*, 70.
3. Murphy, C. Symmetric Missile Dynamic Instabilities. *Journal of Guidance and Control* **1981,** *4*, 464–471.
4. Soper, W. Projectile Instability Produced by Internal Friction. *AIAA Journal* **1978**, *16*, 8–11.
5. Murphy, C. Influence of Moving Internal Parts on Angular Motion of Spinning Projectiles. *Journal of Guidance and Control* **1978**, *1*, 117–122.
6. D'Amico, W. Comparison of Theory and Experiment for Moments Induced by Loose Internal Parts. *Journal of Guidance and Control* **1987**, *10*, 14–19.
7. Hodapp, A. Passive Means for Stabilizing Projectiles With Partially Restrained Internal Members. *Journal of Guidance and Control* **1989**, *12*, 135–139.
8. Schmidt, E.; Donovan, W. Technique to Reduce Yaw and Jump of Fin-Stabilized Projectiles. *Journal of Spacecraft and Rockets* **1998,** *35*, 110–111.
9. Costello, M.; Agarwalla, R. Improved Dispersion of a Fin-Stabilized Projectile Using a Passive Moveable Nose. *Journal of Guidance, Control, and Dynamics* **2000**, *23*, 900–903. Errata: **2002**, *25*, 414.
10. Smith, J.; Smith, K.; Topliffe, R. *Feasibility Study for Application of Modular Guidance and Control Units to Existing ICM Projectiles*; ARLCD-CR-79001; U.S. Army Armament Research and Development Command: Warren, MI, 1978.
11. Costello, M.; Peterson, A. Linear Theory of a Dual Spin Projectile in Atmospheric Flight. *Journal of Guidance, Control, and Dynamics* **2000**, *23*, 789–797.
12. Burchett, B.; Peterson, A.; Costello, M. Prediction of Swerving Motion of a Dual-Spin Projectile With Lateral Pulse Jets in Atmospheric Flight. *Mathematical and Computer Modeling* **2002**, *35*, 821–834.
13. Etkin, B. *Dynamics of Atmospheric Flight*. John Wiley & Sons, Inc.: New York, 1972.
14. Arrow Tech Associates, Inc. *PRODAS*; Burlington, VT, 2002.
15. McCoy, R. L. *Modern Exterior Ballistics*; Schiffer: Atglen, PA, 1999.

INTENTIONALLY LEFT BLANK.

Appendix. Kinetic Differential Equations

Angular velocity of the projectile expressed in the projectile body frame:

$$\vec{\omega}_{P/I} = A_{\omega PP} s \,. \tag{A-1}$$

$$A_{\omega PP} = \left[\begin{array}{c|c|c} \mathrm{O} & \mathrm{I} & \begin{matrix}0\\0\\0\end{matrix} \end{array}\right]. \tag{A-2}$$

$$\mathrm{O} = \begin{bmatrix} 0 & 0 & 0 \\ 0 & 0 & 0 \\ 0 & 0 & 0 \end{bmatrix}, \quad \mathrm{I} = \begin{bmatrix} 1 & 0 & 0 \\ 0 & 1 & 0 \\ 0 & 0 & 1 \end{bmatrix}. \tag{A-3}$$

Angular velocity of the part expressed in the projectile body frame:

$$\vec{\omega}_{D/I} = A_{\omega DP} s \,. \tag{A-4}$$

$$A_{\omega DP} = \left[\begin{array}{c|c|c} \mathrm{O} & \mathrm{I} & U \end{array}\right]. \tag{A-5}$$

$$U = \begin{bmatrix} c_{\theta_D} c_{\psi_D} \\ c_{\theta_D} s_{\psi_D} \\ -s_{\theta_D} \end{bmatrix}. \tag{A-6}$$

Angular velocity of the part expressed in the part body frame:

$$\vec{\omega}_{D/I} = A_{\omega DD} s \,. \tag{A-7}$$

$$A_{\omega DD} = \left[\begin{array}{c|c|c} \mathrm{O} & T_D^T & \begin{matrix}1\\0\\0\end{matrix} \end{array}\right], \tag{A-8}$$

where T_D is the transformation matrix from the part body frame to the projectile body frame:

$$T_D = \begin{bmatrix} c_{\theta_D} c_{\psi_D} & s_{\phi_D} s_{\theta_D} c_{\psi_D} - c_{\phi_D} s_{\psi_D} & c_{\phi_D} s_{\theta_D} c_{\psi_D} + s_{\phi_D} s_{\psi_D} \\ c_{\theta_D} s_{\psi_D} & s_{\phi_D} s_{\theta_D} s_{\psi_D} + c_{\phi_D} c_{\psi_D} & c_{\phi_D} s_{\theta_D} s_{\psi_D} - s_{\phi_D} c_{\psi_D} \\ -s_{\theta_D} & s_{\phi_D} c_{\theta_D} & c_{\phi_D} c_{\theta_D} \end{bmatrix}. \tag{A-9}$$

Angular acceleration of the projectile expressed in the projectile body frame:

$$\vec{\alpha}_{P/I} = A_{\alpha PP}\dot{s}\,. \tag{A-10}$$

$$A_{\alpha PP} = \left[\begin{array}{c|c|c} & & 0 \\ \mathrm{O} & \mathrm{I} & 0 \\ & & 0 \end{array}\right]. \tag{A-11}$$

Angular acceleration of the part expressed in the projectile body frame:

$$\vec{\alpha}_{D/I} = A_{\alpha DP}\dot{s} + B_{\alpha DP}\,. \tag{A-12}$$

$$A_{\alpha DP} = \left[\begin{array}{c|c|c} & & \\ \mathrm{O} & \mathrm{I} & U \\ & & \end{array}\right]. \tag{A-13}$$

$$B_{\alpha DP} = S\{\vec{\omega}_{P/I}\}U\omega\,. \tag{A-14}$$

$S\{\ \}$ designates a skew-symmetric operator formed using the components of the vector it is describing as shown in equation A-15:

$$S\{\ \} = \begin{bmatrix} 0 & -S_3 & S_2 \\ S_3 & 0 & -S_1 \\ -S_2 & S_1 & 0 \end{bmatrix}. \tag{A-15}$$

For instance, $S_{\omega PP}$ is the skew-symmetric operator for the angular velocity of the projectile expressed in the projectile body frame.

Angular acceleration of the part expressed in the part body frame:

$$\vec{\alpha}_{D/I} = A_{\alpha DD}\dot{s} + B_{\alpha DD}\,. \tag{A-16}$$

$$A_{\alpha DD} = T_D^T A_{\alpha DP}\,. \tag{A-17}$$

$$B_{\alpha DD} = T_D^T B_{\alpha DP}\,. \tag{A-18}$$

Translational acceleration of the system reference point expressed in the projectile body frame:

$$\vec{a}_{S/I} = A_{ASP}\dot{s} + B_{ASP}\,. \tag{A-19}$$

$$A_{ASP} = \left[\begin{array}{c|c|c} & & 0 \\ \mathrm{I} & \mathrm{O} & 0 \\ & & 0 \end{array}\right]. \tag{A-20}$$

$$B_{ASP} = S\{\vec{\omega}_{P/I}\}\begin{Bmatrix} u \\ v \\ w \end{Bmatrix}. \tag{A-21}$$

Translational acceleration of the projectile center of mass expressed in the projectile body frame:

$$\vec{a}_{P/I} = A_{APP}\dot{s} + B_{APP}. \tag{A-22}$$

$$A_{APP} = A_{ASP} - S\{\vec{r}_{S\to P}\}A_{\alpha SP}. \tag{A-23}$$

$$B_{APP} = S\{\vec{\omega}_{S/I}\}\begin{Bmatrix} u \\ v \\ w \end{Bmatrix}. \tag{A-24}$$

Translational acceleration of the part expressed in the projectile body frame:

$$\vec{a}_{D/I} = A_{ADP}\dot{s} + B_{ADP}. \tag{A-25}$$

$$A_{ADP} = A_{APP} - S\{\vec{r}_{S\to C}\}A_{\varepsilon PP} - S\{\vec{r}_{C\to D}\}A_{\alpha DP}. \tag{A-26}$$

$$B_{ADP} = B_{APP} + S\{\vec{\omega}_{P/I}\}S\{\vec{\omega}_{P/I}\}\begin{Bmatrix} x_{PC} \\ y_{PC} \\ z_{PC} \end{Bmatrix} - S\{\vec{r}_{C\to D}\}B_{\alpha DP}$$

$$+ S\{\vec{\omega}_{D/I}\}S\{\vec{\omega}_{D/I}\}T_D\begin{Bmatrix} x_{CD} \\ y_{CD} \\ z_{CD} \end{Bmatrix}. \tag{A-27}$$

Translational acceleration of the part expressed in the part body frame:

$$\vec{a}_{D/I} = A_{ADD}\dot{s} + B_{ADD}. \tag{A-28}$$

$$A_{ADD} = T_D^T A_{ADP}. \tag{A-29}$$

$$B_{ADD} = T_D^T B_{ADP}. \tag{A-30}$$

Angular momentum time derivative of the projectile body expressed in the projectile body frame:

$$\frac{d\vec{H}_{P/I}}{dt} = A_{HPP}\dot{s} + B_{HPP}. \tag{A-31}$$

$$A_{HPP} = I_P A_{\alpha PP}. \tag{A-32}$$

$$B_{HPP} = S\{\vec{\omega}_{P/I}\}I_P A_{\omega PP}s. \tag{A-33}$$

Angular momentum time derivative of the part body expressed in the projectile body frame:

$$\frac{d\vec{H}_{D/I}}{dt} = A_{HDP}\dot{s} + B_{HDP}\,. \tag{A-34}$$

$$A_{HDP} = T_D I_D T_D^T A_{\alpha DP}\,. \tag{A-35}$$

$$B_{HDP} = \dot{T}_D I_D T_D^T A_{\alpha DP} s + T_D I_D \dot{T}_D^T A_{\omega DP} s + T_D I_D T_D^T B_{\alpha DP} + S\{\vec{\omega}_{P/I}\} T_D I_D T_D^T A_{\omega DP} s\,. \tag{A-36}$$

Angular momentum time derivative of the part body expressed in the part body frame:

$$\frac{d\vec{H}_{D/I}}{dt} = A_{HDD}\dot{s} + B_{HDD}\,. \tag{A-37}$$

$$A_{HDP} = I_D A_{\alpha DP}\,. \tag{A-38}$$

$$B_{HDP} = I_D B_{\alpha DP} + S\{\vec{\omega}_{D/I}\} I_D A_{\omega DP} s\,. \tag{A-39}$$

Constraint force expressed in the projectile body frame:

$$\vec{F}_R = A_{FRP}\dot{s} + B_{FRP}\,. \tag{A-40}$$

$$A_{FRP} = \frac{m_D m_P}{m_D + m_P}\left(A_{ADP} - A_{APP}\right). \tag{A-41}$$

$$B_{FRP} = \frac{m_D m_P}{m_D + m_P}\left(B_{ADP} - B_{APP} + \frac{1}{m_P}\begin{Bmatrix} X_A \\ Y_A \\ Z_A \end{Bmatrix}\right). \tag{A-42}$$

Translational dynamic equation of motion for the projectile body:

$$A_{PT}\dot{s} = B_{PT}\,. \tag{A-43}$$

$$A_{PT} = m_P A_{APP} + m_D A_{ADP}\,. \tag{A-44}$$

$$B_{PT} = T_P^T \begin{Bmatrix} 0 \\ 0 \\ W_P + W_D \end{Bmatrix} + \begin{Bmatrix} X_A \\ Y_A \\ Z_A \end{Bmatrix} - m_P B_{APP} - m_D B_{ADP}\,. \tag{A-45}$$

Angular dynamic equation of motion for the projectile body:

$$A_{PR}\dot{s} = B_{PR}\,. \tag{A-46}$$

$$A_{PR} = A_{HPP} + A_{HDP} + m_D S\{\bar{r}_{C\to D}\} A_{ADP} + S\{\bar{r}_{P\to C}\} A_{FRP}\,. \tag{A-47}$$

$$B_{PR} = \begin{Bmatrix} L_A \\ M_A \\ N_A \end{Bmatrix} + S\{\vec{r}_{C\to D}\}T_P^T \begin{Bmatrix} 0 \\ 0 \\ W_D \end{Bmatrix} - S\{\vec{r}_{P\to C}\}B_{FRP} - B_{HPP}$$

$$- B_{HDP} - m_D S\{\vec{r}_{C\to D}\}B_{ADP}\,. \tag{A-48}$$

Angular dynamic equation of motion for the part body:

$$A_{DR}\dot{s} = B_{DR}\,. \tag{A-49}$$

$$A_{DR} = \{1 \quad 0 \quad 0\} \bullet [A_{HDD} + m_D S_{RCD} A_{ADD}]. \tag{A-50}$$

$$B_{DR} = \{1 \quad 0 \quad 0\} \bullet \left\{ T_P^T \begin{Bmatrix} 0 \\ 0 \\ W_P + W_D \end{Bmatrix} + \begin{Bmatrix} X_A \\ Y_A \\ Z_A \end{Bmatrix} - m_P B_{APP} - m_D B_{ADP} \right\}. \tag{A-51}$$

INTENTIONALLY LEFT BLANK.

List of Symbols, Abbreviations, and Acronyms

$\vec{a}_{D/I}$	=	Acceleration of unbalanced part mass center with respect to an inertial frame.
$\vec{a}_{P/I}$	=	Acceleration of projectile mass center with respect to an inertial frame.
$\vec{a}_{S/I}$	=	Acceleration of stationary system reference point with respect to an inertial frame.
$\vec{\alpha}_{D/I}$	=	Angular acceleration of unbalanced part with respect to an inertial frame.
$\vec{\alpha}_{P/I}$	=	Angular acceleration of projectile with respect to an inertial frame.
$\vec{F}_A$	=	Aerodynamic forces.
$\vec{F}_R$	=	Reaction force.
$\vec{H}_{P/I}$	=	Angular momentum of the projectile with respect to an inertial frame.
$\vec{H}_{D/I}$	=	Angular momentum of the unbalanced part with respect to an inertial frame.
I_P	=	Mass moment of inertia of the projectile about its mass center.
I_D	=	Mass moment of inertia of the unbalanced part about its mass center.
$\vec{I}_C, \vec{J}_C, \vec{K}_C$	=	Control reference frame unit vectors.
$\vec{I}_D, \vec{J}_D, \vec{K}_D$	=	Unbalanced part frame unit vectors.
$\vec{I}_I, \vec{J}_I, \vec{K}_I$	=	Inertial frame unit vectors.
$\vec{I}_N, \vec{J}_N, \vec{K}_N$	=	No-roll frame unit vectors.
$\vec{I}_P, \vec{J}_P, \vec{K}_P$	=	Projectile frame unit vectors.
L_A, M_A, N_A	=	Total aerodynamic moment components expressed in the body frame.
$\vec{M}_A$	=	Total aerodynamic moment.
$\vec{M}_F$	=	Bearing friction moment.
$\vec{M}_R$	=	Bearing reaction moment.

m_D	=	Unbalanced part body mass.
m_P	=	Projectile mass.
p, q, r	=	Roll, pitch, and yaw components of the angular velocity vector of the projectile expressed in the body frame.
ϕ_C	=	Commanded control angle.
ϕ_E	=	Control angle error.
ϕ_J	=	Part orientation angle.
ϕ, θ, ψ	=	Euler roll, pitch, and yaw angles of projectile.
ϕ_D, θ_D, ψ_D	=	Euler orientation angles of the unbalanced part with respect to the projectile.
$\vec{r}_{C \to D}$	=	Distance from internal part axle connection point to unbalanced part center of mass.
$\vec{r}_{P \to A}$	=	Distance from projectile center of mass to center of pressure.
$\vec{r}_{P \to C}$	=	Distance from projectile center of mass to unbalanced part axle connection point.
$\vec{r}_{P \to D}$	=	Distance from projectile center of mass to unbalanced part center of mass.
$\vec{r}_{P \to M}$	=	Distance from projectile center of mass to center of Magnus force.
$\vec{r}_{S \to P}$	=	Distance from stationary system reference point to projectile center of mass.
$\vec{r}_{S \to C}$	=	Distance from stationary system reference point to unbalanced part axle connection point.
$\vec{T}$	=	Control torque vector.
T_P	=	Transformation matrix from the projectile body frame to the inertial frame.
T_D	=	Transformation matrix from the part body frame to the projectile body frame.
u, v, w	=	Translational velocity components of projectile center of mass resolved in the body frame.

$\vec{V}_{S/I}$	=	Velocity of stationary system reference point with respect to the inertial frame.
$\vec{W}_D$	=	Weight of part body.
$\vec{W}_P$	=	Weight of projectile body.
W_D	=	Magnitude of unbalanced part weight.
W_P	=	Magnitude of projectile body weight vector.
ω	=	Unbalanced part angular velocity component resolved in the unbalanced part frame.
$\vec{\omega}_{D/I}$	=	Angular velocity of unbalanced part with respect to the inertial frame.
$\vec{\omega}_{D/P}$	=	Angular velocity of unbalanced part with respect to the projectile body frame.
$\vec{\omega}_{P/I}$	=	Angular velocity of projectile body with respect to the inertial frame.
X_A, Y_A, Z_A	=	Total aerodynamic force components expressed in the body frame.
x, y, z	=	Position components of the projectile center of mass expressed in the inertial frame.
x_{CD}, y_{CD}, z_{CD}	=	Unbalanced part frame components of distance from part axle connection point to part center of mass.
x_{PC}, y_{PC}, z_{PC}	=	Projectile body frame components of distance from projectile center of mass to part axle connection point.

NO. OF COPIES ORGANIZATION

1 (PDF ONLY) DEFENSE TECHNICAL INFORMATION CTR
DTIC OCA
8725 JOHN J KINGMAN RD
STE 0944
FORT BELVOIR VA 22060-6218

1 US ARMY RSRCH DEV & ENGRG CMD
SYSTEMS OF SYSTEMS INTEGRATION
AMSRD SS T
6000 6TH ST STE 100
FORT BELVOIR VA 22060-5608

1 INST FOR ADVNCD TCHNLGY
THE UNIV OF TEXAS
AT AUSTIN
3925 W BRAKER LN STE 400
AUSTIN TX 78759-5316

1 US MILITARY ACADEMY
MATH SCI CTR EXCELLENCE
MADN MATH
THAYER HALL
WEST POINT NY 10996-1786

1 DIRECTOR
US ARMY RESEARCH LAB
IMNE AD IM DR
2800 POWDER MILL RD
ADELPHI MD 20783-1197

3 DIRECTOR
US ARMY RESEARCH LAB
AMSRD ARL CI OK TL
2800 POWDER MILL RD
ADELPHI MD 20783-1197

3 DIRECTOR
US ARMY RESEARCH LAB
AMSRD ARL CS IS T
2800 POWDER MILL RD
ADELPHI MD 20783-1197

NO. OF COPIES ORGANIZATION

ABERDEEN PROVING GROUND

1 DIR USARL
AMSRD ARL CI OK TP (BLDG 4600)

NO. OF COPIES ORGANIZATION

3 AIR FORCE RSRCH LAB
MUNITIONS DIR
AFRL/MNAV
G ABATE
101 W EGLIN BLVD
STE 219
EGLIN AFB FL 32542

1 CDR WL/MNMF
D MABRY
101 W EGLIN BLVD STE 219
EGLIN AFB FL 32542-6810

20 OREGON STATE UNIVERSITY
DEPT OF MECHL ENGRG
M COSTELLO
CORVALLIS OR 97331

4 CDR
US ARMY ARDEC
AMSTA AR CCH
J DELORENZO
S MUSALI
R SAYER
P DONADIO
PICATINNY ARESENAL NJ
07806-5000

7 CDR
US ARMY TANK MAIN
ARMAMENT SYSTEM
AMCPM TMA
D GUZIEWICZ
R DARCEY
C KIMKER
R JOINSON
E KOPOAC
T LOUZIERIO
C LEVECHIA
PICATINNY ARESENAL NJ
07806-5000

1 CDR
USA YUMA PROV GRND
STEYT MTW
YUMA AZ 85365-9103

1 DIR
BENET LABORATORIES
SMCWV QAR
T MCCLOSKEY
WATERVLIET NY 12189-5000

NO. OF COPIES ORGANIZATION

10 CDR
US ARMY TACOM
AMCPEO HFM
AMCPEO HFM F
AMCPEO HFM C
AMCPM ABMS
AMCPM BLOCKIII
AMSTA CF
AMSTA Z
AMSTA ZD
AMCPM ABMS S W
DR PATTISON
A HAVERILLA
WARREN MI 48397-5000

1 CDR
USAOTEA
CSTE CCA
DR RUSSELL
ALEXANDRIA VA 22302-1458

2 DIR
US ARMY ARMOR CTR & SCHL
ATSB WP ORSA
A POMEY
ATSB CDC
FT KNOX KY 40121

1 CDR
US ARMY AMCCOM
AMSMC ASR A
MR CRAWFORD
ROCK ISLAND IL 61299-6000

2 PROGRAM MANAGER
GROUND WEAPONS MCRDAC
LTC VARELA
CBGT
QUANTICO VA 22134-5000

4 COMMANDER
US ARMY TRADOC
ATCD T
ATCD TT
ATTE ZC
ATTG Y
FT MONROE VA 23651-5000

1 NAWC
F PICKETT
CODE C2774 CLPL
BLDG 1031
CHINA LAKE CA 93555

NO. OF COPIES ORGANIZATION

1 NAVAL ORDNANCE STATION
ADVNCD SYS TCHNLGY BRNCH
D HOLMES
CODE 2011
LOUISVILLE KY 40214-5001

1 NAVAL SURFACE WARFARE CTR
F G MOORE
DAHLGREN DIVISION
CODE G04
DAHLGREN VA 22448-5000

1 US MILITARY ACADEMY
MATH SCI CTR OF EXCELLENCE
DEPT OF MATHEMATICAL SCI
MDN A MAJ DON ENGEN
THAYER HALL
WEST POINT NY 10996-1786

3 DIR
SNL
A HODAPP
W OBERKAMPF
F BLOTTNER
DIVISION 1631
ALBUQUERQUE NM 87185

3 ALLIANT TECH SYSTEMS
C CANDLAND
R BURETTA
R BECKER
7225 NORTHLAND DR
BROOKLYN PARK MN 55428

3 DIR USARL
AMSRL SE RM
H WALLACE
AMSRL SS SM
J EIKE
A LADAS
2800 POWDER MILL RD
ADELPHI MD 20783-1145

1 OFC OF ASST SECY OF ARMY
FOR R&D
SARD TR
W MORRISON
2115 JEFFERSON DAVIS HWY
ARLINGTON VA 22202-3911

2 CDR USARDEC
AMSTA FSP A
S DEFEO
R SICIGNANO
PICATINNY ARESENAL NJ
07806-5000

NO. OF COPIES ORGANIZATION

2 CDR USARDEC
AMSTA AR CCH A
M PALATHINGAL
R CARR
PICATINNY ARESENAL NJ
07806-5000

5 TACOM ARDEC
AMSTA AR FSA
K CHIEFA
AMSTA AR FS
A WARNASCH
AMSTA AR FSF
W RYBA
AMSTA AR FSP
S PEARCY
J HEDDERICH
PICATINNY ARESENAL NJ
07806-5000

5 CDR US ARMY MICOM
AMSMI RD
P JACOBS
P RUFFIN
AMSMI RD MG GA
C LEWIS
AMSMI RD MG NC
C ROBERTS
AMSMI RD ST GD
D DAVIS
RSA AL 35898-5247

3 CDR US ARMY AVN TRP CMD
DIRECTORATE FOR ENGINEERING
AMSATR ESW
M MAMOUD
M JOHNSON
J OBERMARK
RSA AL 35898-5247

1 DIR US ARMY RTTC
STERT TE F TD
R EPPS
BLDG 7855
REDSTONE ARSENAL AL
38598-8052

2 STRICOM
AMFTI EL
D SCHNEIDER
R COLANGELO
12350 RESEARCH PKWY
ORLANDO FL 32826-3276

NO. OF COPIES ORGANIZATION

1 CDR OFFICE OF NAVAL RES
J GOLDWASSER CODE 333
800 N QUINCY ST RM 507
ARLINGTON VA 22217-5660

1 CDR US ARMY RES OFFICE
AMXRO RT IP TECH LIB
PO BOX 12211
RESEARCH TRIANGLE PARK NJ 27709-2211

4 CDR US ARMY AVN TRP CMD
AVIATION APPLIED TECH DIR
AMSATR TI
R BARLOW
E BERCHER
T CONDON
B TENNEY
FT EUSTIS VA 23604-5577

3 CDR NAWC
WEAPONS DIV
CODE 543400D
S MEYERS
CODE C2744
T MUNSINGER
CODE C3904
D SCOFIELD
CHINA LAKE CA 93555-6100

1 CDR NSWC
CRANE DIVISION
CODE 4024
J SKOMP
300 HIGHWAY 361
CRANE IN 47522-5000

1 CDR NSWC
DAHLGREN DIV
CODE 40D
J BLANKENSHIP
6703 WEST HWY 98
PANAMA CITY FL 32407-7001

2 CDR NSWC
J FRAYSEE
D HAGEN
17320 DAHLGREN RD
DAHLGREN VA 22448-5000

NO. OF COPIES ORGANIZATION

5 CDR NSWC
INDIAN HEAD DIV
D GARVICK CODE 40D
L FAN CODE 4110C
V CARLSON CODE 4120
H LAST CODE 4140E
T GRIFFIN CODE 450D
101 STRAUSS AVE
INDIAN HEAD MD 20640-5000

1 CDR NSWC
INDIAN HEAD DIV
LIBRARY CODE 8530
BLDG 299
101 STRAUSS AVE
INDIAN HEAD MD 20640

2 US MILITARY ACADEMY
MATH SCI CTR OF EXCELLENCE
DEPT OF MATHEMATICAL SCI
MDN A
MAJ D ENGEN
R MARCHAND
THAYER HALL
WEST POINT NY 10996-1786

3 CDR US ARMY YUMA PG
STEYP MT AT A
A HOOPER
STEYP MT EA
YUMA AZ 85365-9110

6 CDR NSWC
INDIAN HEAD DIV
CODE 570D J BOKSER
CODE 5710 L EAGLES
J FERSUSON
CODE 57 C PARIS
CODE 5710G S KIM
CODE 5710E S JAGO
101 STRAUSS AVE ELY BLDG
INDIAN HEAD MD 20640-5035

1 BRUCE KIM
MICHIGAN STATE UNIVERSITY
2120 ENGINEERING BLDG
EAST LANSING MI 48824-1226

2 INDUSTRIAL OPERATION CMD
AMFIO PM RO
W MCKELVIN
MAJ BATEMAN
ROCK ISLAND IL 61299-6000

NO. OF COPIES ORGANIZATION

3 PROGRAM EXECUTIVE OFFICER
TACTICAL AIRCRAFT PROGRAMS
PMA 242 1
MAJ KIRBY R242
PMA 242 33
R KEISER (2 CPS)
1421 JEFFERSON DAVIS HWY
ARLINGTON VA 22243-1276

1 CDR NAVAL AIR SYSTEMS CMD
CODE AIR 471
A NAKAS
1421 JEFFERSON DAVIS HWY
ARLINGTON VA 22243-1276

3 ARROW TECH ASSOCIATES INC
R WHYTE
A HATHAWAY
H STEINHOFF
1233 SHELBOURNE RD SUITE D8
SOUTH BURLINGTON VT 05403

3 US ARMY AVIATION CTR
DIR OF COMBAT DEVELOPMENT
ATZQ CDM C
B NELSON
ATZQ CDC C
T HUNDLEY
ATZQ CD
G HARRISON
FORT RUCKER AL 36362

ABERDEEN PROVING GROUND

3 CDR
USA ARDEC
AMSTA AR FSF T
R LIESKE
J WHITESIDE
J MATTS
BLDG 120

1 CDR
USA TECOM
AMSTE CT
T J SCHNELL
RYAN BLDG

3 CDR
USA AMSAA
AMXSY EV
G CASTLEBURY
R MIRABELLE
AMXSY EF
S MCKEY

NO. OF COPIES ORGANIZATION

44 DIR USARL
AMSRD ARL WM
T ROSENBERGER
AMSRD ARL WM BA
W HORST JR
W CIEPELLA
F BRANDON
T BROWN (5 CPS)
L BURKE
J CONDON
B DAVIS
T HARKINS (5 CPS)
D HEPNER
V LEITZKE
M HOLLIS
A THOMPSON
G BROWN
AMSRD ARL WM BB
B HAUG
AMSRD ARL WM BC
P PLOSTINS (4 CPS)
G COOPER
B GUIDOS
J SAHU
M BUNDY
D LYON
AMSRD ARL WM BC
J BENDER
J GARNER
S WILKERSON
W DRYSDALE
R COATES
A MIKHAL
J WALL
AMSRD ARL WM BD
B FORCH
AMSRD ARL WM BE
M SCHMIDT
AMSRD ARL WM BF
AMSRD ARL WM BR
C SHOEMAKER
J BORNSTEIN